https://doi.org/10.5194/egusphere-2024-2240
Preprint. Discussion started: 30 July 2024

Dynamics of stratospheric wave reflection over the North Pacific

Michael K. Schutte[1], Alice Portal[2], Simon H. Lee[3], and Gabriele Messori[1,4,5]

[1]Department of Earth Sciences, Uppsala University, Uppsala, Sweden
[2]Institute of Geography, Oeschger Centre for Climate Change Research, University of Bern, Bern, Switzerland
[3]School of Earth and Environmental Sciences, University of St Andrews, St Andrews, UK
[4]Swedish Centre for Impacts of Climate Extremes, Uppsala University, Uppsala, Sweden
[5]Department of Meteorology and Bolin Centre for Climate Research, Stockholm University, Stockholm, Sweden

Correspondence: Michael Schutte (michael.schutte@geo.uu.se)

Abstract. Stratospheric wave reflection events involve the upward propagation of planetary waves, which are subsequently reflected downward by the stratospheric polar vortex. This phenomenon establishes a connection between the large-scale circulations in the troposphere and in the stratosphere. Here, we investigate wave reflection events characterised by an enhanced difference between poleward eddy heat flux over the Northwest Pacific and equatorward eddy heat flux over Canada. Previous research has pointed to a link between these events and anomalies in the tropospheric circulation over North America, with an associated abrupt continental-scale surface temperature decrease over the same region. In this study, we aim to elucidate the dynamical mechanisms governing this chain of events.

We find that anomalies of meridional eddy heat flux over the Northwest Pacific and Canada change sign before and after reflection events. A westward-propagating ridge, associated with a positive geopotential height anomaly, and the development of a trough downstream can explain this sign change. The trough advects colder-than-average air southwards in the lower troposphere over North America, leading to an abrupt temperature decrease close to the surface. This corresponds in the upper troposphere to negative and in the lower troposphere to positive anomalies of meridional eddy heat flux. The evolution of this large-scale pattern resembles the shift from a Pacific Trough to an Alaskan Ridge weather regime. Furthermore, stratospheric wave reflection events exert a far-reaching influence beyond North America on the tropospheric circulation across the Northern mid- and high latitudes. One example is the zonalisation and intensification of the North Atlantic eddy-driven jet stream resulting in more frequent occurrences of windy extremes over Europe a few days after the temperature decrease across North America.

https://doi.org/10.5194/egusphere-2024-2240
Preprint. Discussion started: 30 July 2024

1 Introduction

The variability of the stratospheric polar vortex plays a crucial role in shaping tropospheric circulation patterns and influencing weather extremes on subseasonal to seasonal timescales (Baldwin and Dunkerton, 2001; Thompson and Wallace, 2001; Domeisen and Butler, 2020; Kodera et al., 2013; Afargan-Gerstman et al., 2020). One notable example is that of sudden stratospheric warmings (SSWs), characterised by a rapid temperature increase in the stratosphere over the polar regions and a disruption of the stratospheric polar vortex (Scherhag, 1952; Matthewman et al., 2009; Charlton and Polvani, 2007). The occurrence of SSWs is favored by upward propagation of Rossby waves from the troposphere, which break in the stratospheric westerlies and weaken them (Matsuno, 1971; Sjoberg and Birner, 2012; Polvani and Waugh, 2004; Reichler and Jucker, 2022), although enhanced tropospheric wave activity is neither a necessary nor a sufficient condition for the occurrence of an SSW (de la Cámara et al., 2019; Birner and Albers, 2017; Albers and Birner, 2014). The study of SSWs has received particular attention due to their potential to modulate the tropospheric circulation (Charlton-Perez et al., 2018; Hitchcock and Simpson, 2014) and hence surface weather; for example, by favouring large-scale cold-air outbreaks over Eurasia (Cohen et al., 2007; Kretschmer et al., 2018; Kidston et al., 2015).

A related but distinct phenomenon, stratospheric wave reflection, has been linked to cold-air outbreaks over North America (Millin et al., 2022; Kodera et al., 2016; Kretschmer et al., 2018; Messori et al., 2022; Matthias and Kretschmer, 2020; Guan et al., 2020). Stratospheric wave reflection events are characterized by a local maximum of zonal winds in the mid-stratosphere (Perlwitz and Harnik, 2004; Messori et al., 2022) and imply the downward reflection of upward-propagating Rossby waves from the troposphere (Harnik and Lindzen, 2001; Perlwitz and Harnik, 2003; Shaw et al., 2010; Shaw and Perlwitz, 2013). There is no clear consensus on the definition of stratospheric wave reflection events. Some studies focus on daily wave activity fluxes (Plumb, 1985; Kodera et al., 2008; Nath et al., 2014) or zonal-mean wave geometry diagnostics (Harnik and Lindzen, 2001; Shaw et al., 2010; Shaw and Perlwitz, 2013), which are insightful but computationally intensive and may require data that are usually not a standard output of reanalysis products or climate models (Matthias and Kretschmer, 2020). Another approach uses a reflection index based on the difference in zonal-mean zonal winds at 2 and 10 hPa (Perlwitz and Harnik, 2003; Harnik, 2009; Nath et al., 2016), but this index cannot distinguish between SSWs and reflection events (Harnik, 2009). Alternatively, meridional eddy heat flux can be used to detect stratospheric wave reflection, since it is proportional to the vertical component of the Eliassen-Palm (EP) flux which, according to linear wave theory, indicates the vertical group velocity. Earlier studies have connected extremes of the zonal mean meridional eddy heat flux in the stratosphere to changes in stratospheric and tropospheric circulation (Dunn-Sigouin and Shaw, 2015; Shaw et al., 2014; Polvani and Waugh, 2004). However, due to the use of zonal averaging, these methods identify wave reflection events in time but not in space.

To overcome this challenge, Matthias and Kretschmer (2020) proposed an index based on regional averages of the meridional eddy heat flux that is able to capture wave reflection events over the North Pacific. This index is motivated by the average pattern of the meridional eddy heat flux, which consists of positive vertical Rossby-wave group velocity over the Bering strait and negative group velocity over North Canada. Previous research has highlighted that this definition of stratospheric wave reflection captures events leading to a significant decrease in 2m air temperatures over North America and a transition

https://doi.org/10.5194/egusphere-2024-2240
Preprint. Discussion started: 30 July 2024

from the Pacific Trough (PT) to the Alaskan Ridge (AKR) North American weather regime (Messori et al., 2022; Matthias and Kretschmer, 2020; Cohen et al., 2022). However, the physical mechanisms linking stratospheric wave reflection to the subsequent tropospheric anomalies are not completely understood.

In this work, we aim to provide a deeper insight into the evolution of the atmosphere during and after reflection events over the North Pacific, with a particular focus on weather regimes over North America. We specifically seek to answer the following research questions:

1. What is the vertical structure of the meridional eddy heat flux before, during and after reflection events?
2. How does Rossby wave activity change throughout reflection events and how is this change associated with the shift from PT to AKR regimes?
3. Do reflection events over the North Pacific affect the mid-latitude circulation beyond North America?

To address these questions, we first analyze the evolution of reflection events with respect to meridional eddy heat flux and geopotential height anomalies. We further compare changes in geopotential height during reflection events to the shift from PT to AKR regimes. Furthermore, we investigate changes in the mid-latitude tropospheric Rossby wave activity through space-time spectral analysis. In contrast to analyses focusing on circulation indices (Baldwin and Dunkerton, 2001; Thompson et al., 2006; Hall et al., 2021; Kolstad et al., 2022), or weather regimes (Charlton-Perez et al., 2018; Domeisen et al., 2020; Hall et al., 2023; Messori et al., 2022; Lee et al., 2022), this allows to study time-varying wave structures with different horizontal scales and phase speeds. Previous studies have already employed such a methodology to compare Rossby wave properties across data sets (Dell'Aquila et al., 2005) and time periods (Riboldi et al., 2020; Sussman et al., 2020). Furthermore, the method has been proved useful to analyse circumpolar Rossby wave patterns during boreal winter (Riboldi et al., 2022) and the connection between the stratosphere and troposphere during strong and weak stratospheric polar vortex events (Schutte et al., 2024).

https://doi.org/10.5194/egusphere-2024-2240
Preprint. Discussion started: 30 July 2024

2 Methods

2.1 Data

The analysis is based on ERA5 reanalysis data (Hersbach et al., 2020) with a spatial resolution of $1^\circ \times 1^\circ$ and daily temporal resolution, covering the extended winter season (DJFM) from 1 December 1979 to 31 March 2021. We analyse geopotential height, zonal and meridional wind, daily maximum of hourly 10-m wind speed, and air temperature. Space-time Rossby wave spectra are obtained from the meridional wind at $0.75^\circ \times 0.75^\circ$ and 6 hourly resolution. We deseasonalised each dataset, except the meridional wind, by subtracting the daily seasonal cycle, computed with a 15-day centred running mean using data from 16 November to 15 April. Additionally, the temperature field is linearly detrended to account for global warming. The wave activity flux (WAF) is calculated following Plumb (1985) using the NCL script provided in Nishii (2016).

2.2 Event definition

To identify reflection events, we follow the procedure outlined in Messori et al. (2022). Firstly, deviations from the zonal mean of meridional wind and air temperature are multiplied together to obtain the meridional eddy heat flux, $v'T'$. Next, we compute the regional cosine-latitude weighted averages of $v'T'$ over the Siberian domain (45-75°N, 140-200°E) and the Canadian domain (45-75°N, 230-280°E), shown in Fig. A1. These averages are then standardized by removing the daily mean and subsequently dividing by the standard deviation for each calendar day, as indicated by asterisks. The reflection index is:

$$RI = (v'T')^*_{Sib} - (v'T')^*_{Can} \tag{1}$$

We identify stratospheric reflection events when RI exceeds a value of 1 for a minimum of 10 consecutive days, yielding 45 events during the months of December to March (DJFM). Each event can be assigned either to its onset or to its end date. Previous studies have investigated the sensitivity of this definition to parameter choice (e.g. Matthias and Kretschmer, 2020; Messori et al., 2022).

The relationship between wave reflection events and the large-scale circulation over North America is investigated using the weather regime data provided by Lee et al. (2023b). This dataset contains five year-round weather regimes defined over North America (20-80°N, 180-330°E) through a k-means cluster analysis of 10-day low-pass filtered 500 hPa geopotential height fields. The five regimes are Pacific Trough (PT), Pacific Ridge (PR), Alaskan Ridge (AKR), Greenland High (GH), and No Regime (N). Further details of the regime classification can be found in Lee et al. (2023a). We then define North American weather regime 'events' as instances of more than 5 consecutive days with the same regime. Applying this criterion, we identified 91 events for AKR and 107 events for PT, with the central date considered as the event date. We further define a PT-to-AKR transition when the PT regime is present on at least one of the 15 days preceding an AKR event. Using this definition, we identified 62 such transition events with day 0 set as the midpoint of the AKR event. The corresponding large-scale patterns are qualitatively independent of the choice of thresholds.

https://doi.org/10.5194/egusphere-2024-2240
Preprint. Discussion started: 30 July 2024

To verify whether the hemispheric-scale space-time Rossby wave decomposition reflects the dynamics of North Pacific reflection events, we define a regionalized signal of reflection events. We specifically select days where the cosine-latitude weighted spatial correlation of 100 hPa geopotential height anomalies over 45°N to 75°N and 140°E to 80°W (purple box in Fig. A1) with the composite anomalies during reflection events exceeds 0.95. We compute regionalized events separately for the onset and end dates of the reflection events using the Pearson correlation coefficient. Subsequently, we merge high-correlation days that are separated by less than 10 days to one regionalized event by selecting the day with the highest correlation coefficient at 100 hPa as the regionalized event date. This gives 63 regionalized events with geopotential height anomalies correlated to the onset of reflection events and 54 events correlated to the end of reflection events.

2.3 Space-time Rossby wave spectra

Space-time wave spectra decompose a time-varying wave structure (as illustrated, for example, in an Hovmöller diagram) into distinct harmonics with varying horizontal scales and phase speeds. We obtain the space-time spectra of Rossby waves following the procedure described in Riboldi et al. (2022); Schutte et al. (2024). Rossby waves, represented by meridional wind between 35°N and 75°N, are decomposed in time and in space along each latitude circle using a double Fourier transform:

$$V(\lambda,t;\phi) = \sum_{j=-N_T/2}^{N_T/2} \sum_{n=-N_L/2}^{N_L/2} \hat{V}(n,\omega_j;\phi)\, e^{i(n\lambda-\omega_j t)}, \tag{2}$$

where $\hat{V}(n,\omega_j;\phi)$ denotes the complex Fourier coefficient for a given wavenumber n, angular frequency ω_j and latitude ϕ of the meridional wind $V(\lambda,t;\phi)$ at longitude λ, time t and latitude ϕ. The number of grid points along a given latitude circle is $N_L = 480$, and $\omega_j = 2\pi j/N_T$ is the angular frequency, with $N_T = 244$ six-hourly time steps over 61 days. For the decomposition in time, each day is treated as the midpoint of a sliding 61-day time frame, centered at 12 UTC. To minimize boundary effects, a double cosine tapering method is applied, smoothing out the first and last 12 days of each window. This yields periodograms $\mathrm{S}_{\overline{\mathrm{V'V'}}}(n,\omega_j;\phi) = 2\,Re(\hat{V}\hat{V}^*)$ as a function of frequency and wavenumber, where $\hat{V}^*$ is the complex conjugate of the corresponding coefficient $\hat{V}$ and the overline denotes the absolute value of the spectrum. Each periodogram undergoes ten iterations of smoothing in the frequency direction, employing a three-point window, as in Wheeler and Kiladis (1999). Subsequently, these periodograms are remapped to the phase speed domain along each latitude circle by interpolating the periodogram along lines of constant phase speed $c_p = \omega/k$, followed by re-scaling (Randel and Held, 1991). After averaging in the latitude band between 35°N and 75°N, one obtains the spectra $\mathrm{S}_{\overline{\mathrm{V'V'}}}(n,c_p)$. As for the other variables, the spectra are deseasonalised by subtracting the daily seasonal cycle, computed with a 15-day centred running mean using data from 16 November to 15 March. Further details can be found in the Supplement to Riboldi et al. (2022).

Based on the space-time spectra obtained, two integral metrics can be defined to summarize the overall magnitude of Rossby wave activity and the direction of wave propagation. Firstly, the integrated spectral power (ISP) as a measure of the overall magnitude of spectral density of Rossby waves across all wavenumbers n and phase speeds c_p:

https://doi.org/10.5194/egusphere-2024-2240
Preprint. Discussion started: 30 July 2024

$$\mathrm{ISP} = \sum_{n=1}^{15} \sum_{c_p=-30}^{30} S(n, c_p) \tag{3}$$

To obtain the ISP of westward-propagating Rossby waves, one can integrate between phase speeds from -30 ms^{-1} to 0 ms^{-1}. We denote this as ISP_{west} and, analogously, ISP_{east} for the ISP of Rossby waves with positive phase speeds integrated between 0 ms^{-1} and 30 ms^{-1}.

Secondly, the Rossby wave phase speed $\overline{c_p}$, defined in Riboldi et al. (2020), serves as a hemispherically-averaged estimate across the resolved harmonics and represents a weighted mean:

$$\overline{c_p} = \frac{\sum_{n=1}^{15}\sum_{c_p=-30}^{30} \mathrm{S}_{\overline{\mathrm{V'V'}}}(n, c_p) \cdot c_p}{\sum_{n=1}^{15}\sum_{c_p=-30}^{30} \mathrm{S}_{\overline{\mathrm{V'V'}}}(n, c_p)} = \frac{1}{\mathrm{ISP}} \sum_{n=1}^{15} \sum_{c_p=-30}^{30} \mathrm{S}_{\overline{\mathrm{V'V'}}}(n, c_p) \cdot c_p \tag{4}$$

The phase speed associated with each (n, c_p) harmonic is weighted by the corresponding spectral energy density $\mathrm{S}_{\overline{\mathrm{V'V'}}}(n, c_p)$, ensuring that the harmonics most active during each time period contribute more to the overall value of $\overline{c_p}$.

2.4 Significance assessment

The significance of composite anomalies, such as those indicated by hatching in Fig. 1 is assessed using 10 000 bootstrapping iterations (i.e., random sampling with replacement). Following the approach by Wilks (2016), we correct the significance assessment to account for multiple testing. Indeed, for a given geographical map, a large number of tests are conducted (e.g. $N_{tests} = N_{lat} \cdot N_{lon} \approx 20\ 000$), and hence the risk of erroneously deeming a point significant solely by chance is high. Following equation (3) in Wilks (2016), we look for the largest percentile p^*_{FDR} that satisfies the condition:

$$p^*_{FDR} = max_{i=1\ldots N}[p_i \ : \ p_i \leq (\frac{i}{N}) \cdot \alpha_{FDR}], \tag{5}$$

where N represents the number of significance tests, and p_i is the i-th entry in the sorted list of percentile. Given the spatial and temporal correlation between data points, the chosen control level α_{FDR} is set to 0.10 (Wilks, 2016). Consequently, p^*_{FDR}, which in our analyses yields mostly values below 0.05, is selected as the new significance level.

https://doi.org/10.5194/egusphere-2024-2240
Preprint. Discussion started: 30 July 2024

3 Results

3.1 Evolution of stratospheric reflection events

3.1.1 Temporal and spatial patterns in meridional eddy heat flux

Following the definition of reflection events from Sect.2.2, the difference between $v'T'$ anomalies in the Siberian domain and the Canadian domain is maximised during reflection events. This corresponds to positive $v'T'$ anomalies and enhanced upward-propagating Rossby waves over Siberia and negative $v'T'$ anomalies and enhanced downward-propagating Rossby waves over Canada.

The positive anomalies over Siberia during reflection events are preceded by negative anomalies with a distinct vertical structure. Both the negative and positive $v'T'$ anomalies reach down into the upper troposphere, but the positive anomalies are strongest in the stratosphere (Fig. 1 a). The lack of significant anomalies below 300 hPa could arise from greater tropospheric variability during reflection events. Furthermore, when centered around the reflection onset date, significant positive anomalies in $v'T'$ start four days earlier in the middle stratosphere (10 hPa) compared to the upper troposphere (200 hPa) (Fig. 1 a). This highlights the stratospheric onset of reflection events, connected to a local vertical maximum of zonal wind speeds at 10 hPa, which plays a crucial role in pre-conditioning the stratosphere for wave reflection events (cf. Fig. 2 in Messori et al. (2022)). When centered around the end date, additional negative anomalies of Siberian $v'T'$ emerge (1 b).

The alternation of different signed $v'T'$ anomalies around reflection events is also evident in the Canadian domain (Fig. 1 c and d). Here, a more pronounced coupling to lower tropospheric levels is discernible, although most of the significant signal is above 300 hPa. When centered around the end of reflection events, positive $v'T'$ anomalies emerge close to the surface around lag -8 days, later extending to higher levels (Fig. 1 d). The emergence of low-level positive $v'T'$ anomalies is possibly connected to the southward advection of colder-than-average air near the surface. At the same time, the negative upper-level anomalies weaken from higher stratospheric levels downward, consistent with decreasing wave reflection and increasing Rossby wave breaking in the middle stratosphere. This leads to anomalies of opposite sign at upper and lower levels in the days preceding the end of the reflection events.

To better understand this vertical structure, we consider the spatiotemporal evolution of $v'T'$ around the end of the reflection events, designated as day 0. The $v'T'$ anomalies in the stratosphere and upper troposphere show a clear oscillation over time in both the Siberian and Canadian domains. During the peak of reflection events, the 100 hPa anomalies remain mostly confined within these domains. However, the negative $v'T'$ anomaly above Canada starts to propagate westward around day 0 (Fig. 2 a). An additional positive anomaly emerges within the Canadian domain at lags +5 to +12 days. Additional positive anomalies of meridional eddy heat flux during reflection events are evident over Asia and Europe, suggesting a possible connection between reflection events and hemispheric-scale circulation patterns. Anomalies in the upper troposphere mirror the behaviour of the lower stratosphere, albeit with weaker anomalies (Fig. 2 b), as also seen in Fig. 1.

The picture at 850 hPa is very different compared to the upper levels, notably in the positive anomalies that emerge in the Canadian domain at negative lags of a few days (Fig. 2 c). These correspond to the southward advection of colder-than-average

https://doi.org/10.5194/egusphere-2024-2240
Preprint. Discussion started: 30 July 2024

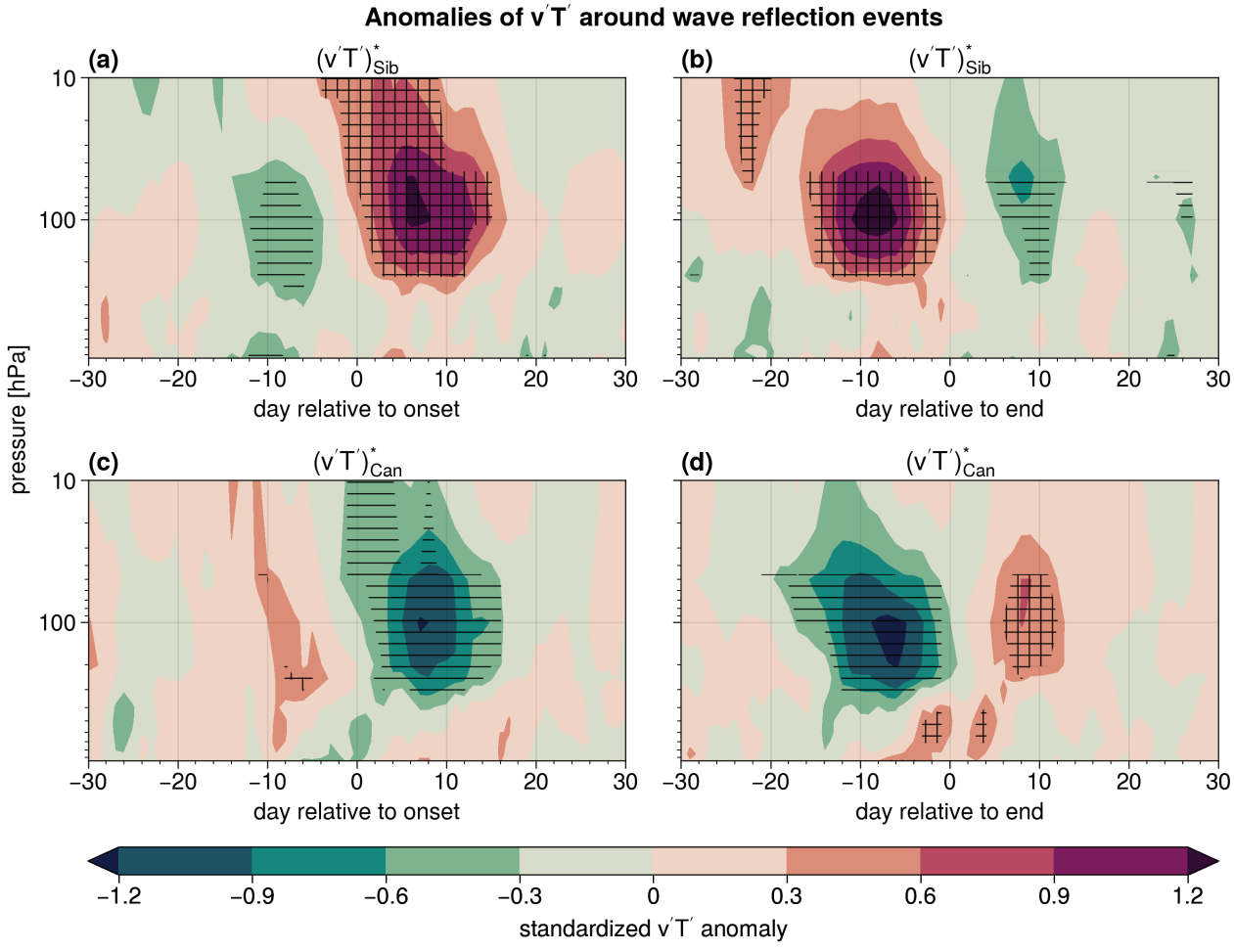

Figure 1. Vertical cross-section of standardized anomalies of composite meridional eddy heat flux $v'T'$ averaged over the Siberian domain (45-75°N, 140-200°E) around (a) onset date and (b) end date of reflection events. In panels (c) and (d) the same is shown for the Canadian domain (45-75°N, 230-280°E). Horizontal hatching marks significant negative anomalies and cross-hatching significant positive anomalies.

air, associated with negative 2m air temperature anomalies (Fig. 2 c). This stands in stark contrast to the positive temperature anomalies around the onset of the reflection events, associated with positive $v'T'$ anomalies over the Northeast Pacific which correspond to northward warm air advection. Investigating the evolution of air temperature anomalies confirms the similar behaviour between the two upper levels, which differs from the behaviour at 850 hPa (Fig. A2).

In summary, the majority of significant $v'T'$ anomalies are observed in the upper troposphere and stratosphere during reflection events. The oscillation of $v'T'$ anomalies in the Siberian and Canadian domain originates from the westward propagation of negative $v'T'$ anomalies and the subsequent formation of new positive $v'T'$ anomalies downstream. In the Canadian domain, positive anomalies are also evident at lower tropospheric levels a few days before the end of the reflection events, exhibiting

https://doi.org/10.5194/egusphere-2024-2240
Preprint. Discussion started: 30 July 2024

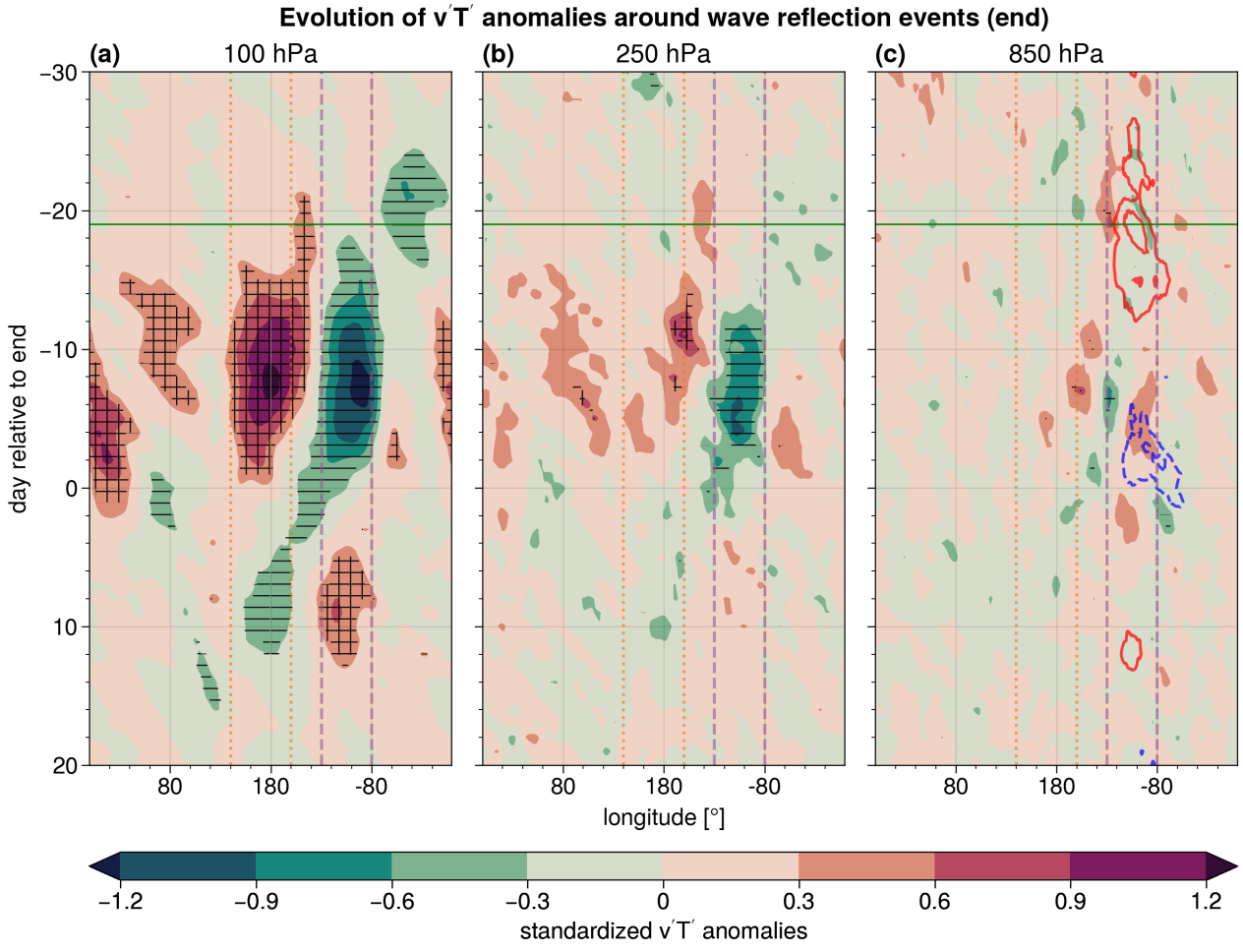

Figure 2. Hovmöller diagram of standardized anomalies of composite meridional eddy heat flux $v'T'$ averaged between 45°N - 75°N centered around the end date of reflection events at (a) 100 hPa, (b) 250 hPa and (c) 850 hPa. Horizontal hatching marks significant negative anomalies and cross-hatching significant positive anomalies. Continuous red and dashed blue contours in (c) show standardized positive and negative 2m air temperature anomalies, respectively, averaged between 40°N - 55°N ($1\ std \approx 3.8\ K$). The contours start at $\pm 0.5 std$ with steps of $0.3 std$. The continuous horizontal green line shows the median onset day of reflection events. The vertical lines mark longitudes of the Siberian (orange, dotted) and Canadian domains (purple, dashed).

an opposite sign to upper levels at that time. These positive, low-level $v'T'$ anomalies correspond to a large-scale decrease in 2m air temperatures during reflection events.

https://doi.org/10.5194/egusphere-2024-2240
Preprint. Discussion started: 30 July 2024

3.1.2 Evolution of geopotential height anomalies

After highlighting westward-propagating $v'T'$ anomalies around the end of reflection events, we now connect this behaviour to the evolution of geopotential height anomalies and WAF.

A westward propagating ridge stands out as a characteristic feature of reflection events. The positive geopotential height anomaly associated with the ridge forms during the onset at 100 hPa over the Canadian domain (Fig. 3 a). This anomaly intensifies and exhibits westward propagation as the events progress, reaching Europe by day +6. Shortly after the formation of the ridge, a trough forms over Eurasia and persists throughout the duration of the reflection events. After the end of the event, a new trough develops over North America, downstream of the westward propagating ridge. West of the ridge, upward WAF anomalies match the positive $v'T'$ anomalies observed over the Siberian domain (cf. Figs. 2 a and 3 a), and exhibit a stronger-than-average eastward component from day -15 to 0. Enhanced downward WAF east of the ridge corresponds to the negative anomalies of $v'T'$ over North America. The behaviour of geopotential height and WAF at 250 hPa closely resembles that observed at 100 hPa, albeit with slightly weaker anomalies (Fig. 3 b). While the significant strengthening of the ridge at 250 hPa occurs a few days later than at 100 hPa, the negative geopotential height anomaly downstream of the ridge precedes that at 100 hPa by a few days (cf. Fig. 3 a and b).

As in the case of the $v'T'$ anomalies, the pattern of geopotential and WAF anomalies is different at lower levels. Downward 850 hPa WAF anomalies over North America around the onset of reflection events are replaced, around day -10, by enhanced upward and eastward anomalies (Fig. 3 c). The mid-tropospheric convergence of WAF occurring before the end of reflection events has been connected to the emergence of a trough over Canada by Millin et al. (2022). At the same time, the geopotential height anomalies propagate to the west and replace the negative anomaly over the North Pacific, similarly to the upper levels. The downstream development of the negative 850 hPa geopotential height anomaly occurs at around -10 days, earlier than at upper levels.

The westward propagation of the ridge around the end of reflection events corresponds to increasing ISP for Rossby waves with westward phase speed (Fig. 3 d). The reflection events exhibit initially suppressed values of ISP_{west} after the median onset day, followed by a roughly monotonic increase until a few days before their end. The spectral properties of Rossby waves are further analysed in Section 3.1.3.

The evolution of the spatial pattern of geopotential height anomalies highlights the hemispheric scale of the reflection events (Fig. 4). In addition to the westward-propagating ridge and subsequent development of a trough downstream, consistent with Fig. 3, we also observe clear geopotential height anomalies over Eurasia (first three columns in Fig. 4). Specifically, a Rossby wave train pattern extending from the North Atlantic to East Siberia suggests a hemispheric-scale circulation pattern around the end of reflection events (Fig. 4 c and h). This pattern, as well as the shift of geopotential height anomalies over North America and the Pacific, are even more pronounced when contrasting reflection event onset and end (Fig. 4 d and i). Furthermore, the evolution in geopotential height anomalies is coherent between 100 hPa and 850 hPa (Fig. A3), highlighting the largely barotropic character of reflection events.

https://doi.org/10.5194/egusphere-2024-2240
Preprint. Discussion started: 30 July 2024

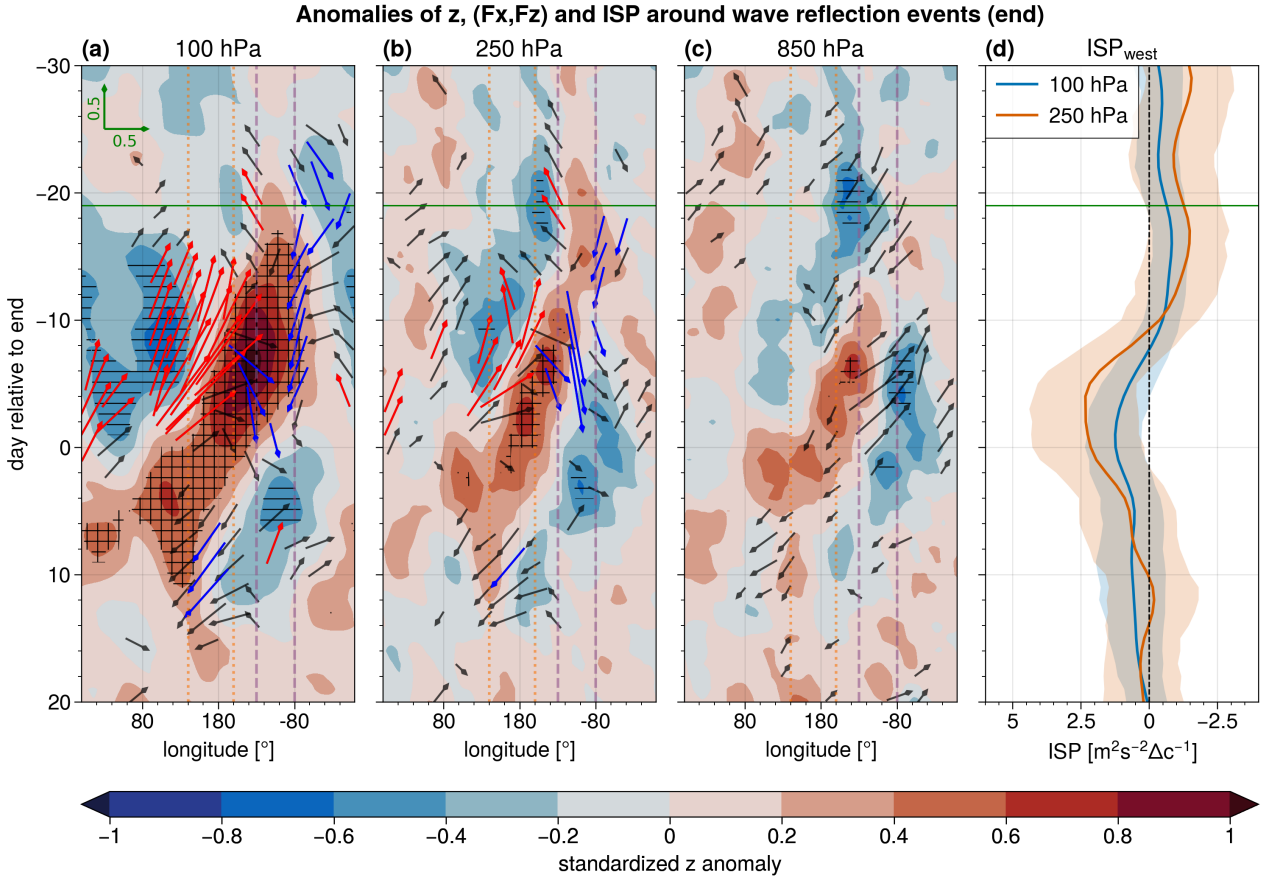

Figure 3. Hovmöller diagram of standardized anomalies of geopotential height averaged between 45°N - 75°N centered around the end date of reflection events at (a) 100 hPa, (b) 250 hPa and (c) 850 hPa in shading. Horizontal hatching marks significant negative anomalies and cross-hatching significant positive anomalies. Arrows indicate anomalies of the zonal and vertical component of WAF (Plumb, 1985) (blue: significantly negative vertical component, red: significantly positive vertical component). Only values larger than 0.1 std are shown. (d) Time series of ISP for westward-propagating Rossby waves and the 95% confidence interval (shaded area) at 100 hPa and 250 hPa. The continuous horizontal green line shows the median onset time of reflection events. The vertical lines mark longitudes of the Siberian (orange, dotted) and Canadian domains (purple, dashed).

The temperature anomalies associated with the ridge formation over the North Pacific align with the previously discussed $v'T'$ anomalies. Warm air is advected northward at higher levels over the North Pacific around the ridge and redirected southward over North America (Fig. 4 e). The temperature anomalies at lower levels exhibit a more distinct pattern than at 100 hPa, with warmer-than-average air predominantly directed poleward over Alaska around day -4 (Fig. 4 j).

In summary, the onset of reflection events is characterised by a vertically coherent positive geopotential height anomaly at upper levels over North Canada. This propagates westward, reaching Siberia by the end of the events. At the same time, a

https://doi.org/10.5194/egusphere-2024-2240
Preprint. Discussion started: 30 July 2024

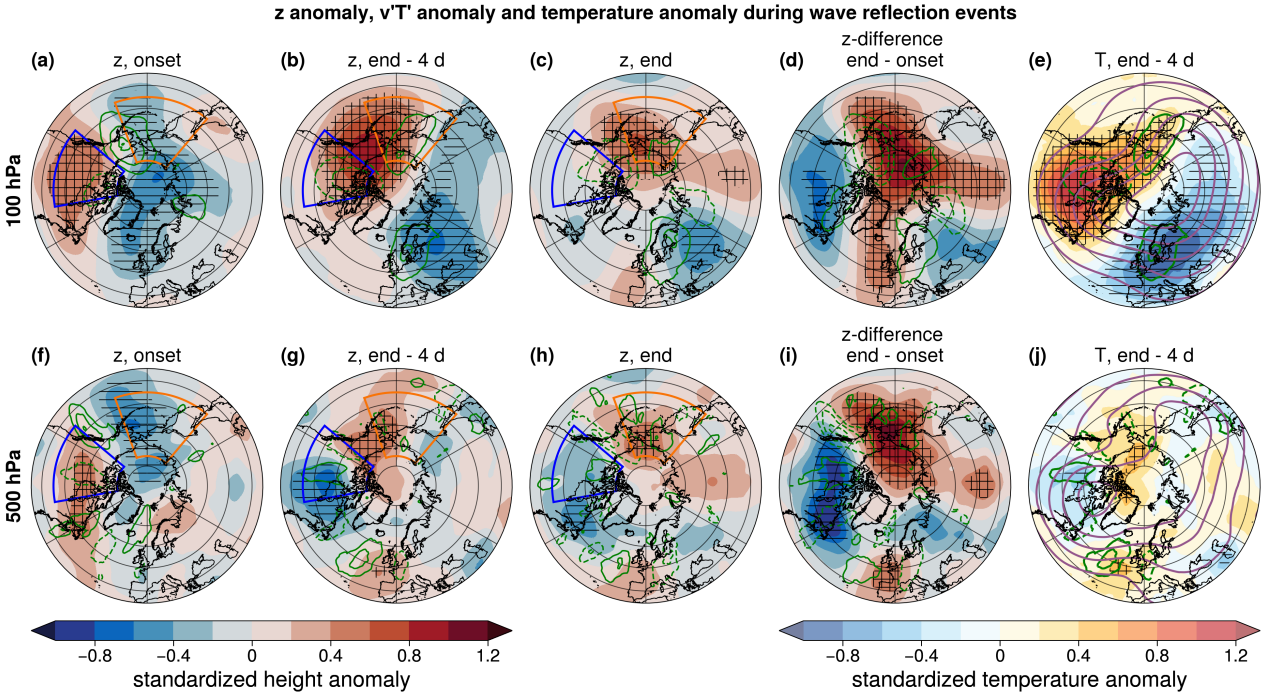

Figure 4. Geopotential height anomalies in shading and $v'T'$ anomalies in green contours (a, f) during onset, (b, g) 4 days before end, (c, h) at the end date and (d, i) difference between onset and end of reflection events at 100 hPa (first row) and 500 hPa (second row). Horizontal hatching marks significant negative geopotential height anomalies and cross-hatching significant positive anomalies. (e, j) Temperature anomalies in shading, geopotential height field in purple and $v'T'$ anomalies in green 4 days before end.

negative geopotential height anomaly emerges downstream over eastern Canada, first at lower levels and later extending into the stratosphere. At upper levels enhanced upward WAF is observed over the Siberian domain west of the ridge, and enhanced downward WAF over Canada east of the ridge. Positive WAF anomalies close to the surface over North America emerge 10 days before the end of reflection events.

https://doi.org/10.5194/egusphere-2024-2240
Preprint. Discussion started: 30 July 2024

3.1.3 Rossby wave characteristics during reflection events

We next leverage space-time spectral analysis, described in Section 2.3, to investigate the Rossby wave behaviour at the onset and end of reflection events.

Rossby wave spectra indicate an enhancement of westward-propagating Rossby waves from the onset to the end of reflection. During the onset at 100 hPa, eastward-propagating waves 2 to 5 are amplified and westward-propagating waves are damped, suggesting the presence of an accelerated stratospheric flow (Fig. 5 a). This is followed by higher activity for westward-propagating Rossby waves during the end of the events, which agrees with the above findings regarding westward-propagating anomalies (Fig. 5 b). The deceleration of Rossby waves during the evolution of the reflection events is characterised by a significant enhancement of westward-propagating wave 1 and 3+ and by a decreased activity for eastward-propagating waves 2 to 4 (Fig. 5 c). The higher wavenumber anomalies lie in a phase-space region with low spectral power. Although they contribute less to the overall Rossby wave energy and to the formation of troughs and ridges, they further support the presence of increased activity for retrograding Rossby waves at the end of reflection events. The upper troposphere displays a similar pattern to the stratosphere, albeit with a weaker change in the westward-propagating wave-1 (Fig. 5 d to f). Finally, westward-propagating Rossby wave activity increases also at stratospheric levels above 100 hPa (Fig. A4).

The phase speed of Rossby waves in the vertical column between 850 hPa and 10 hPa thus decreases during the course of reflection events (Fig. 6 a). Higher phase speed $\overline{c_p}$ in the lower stratosphere and troposphere around the onset of reflection events could indicate a faster zonal flow, in line with enhanced activity of eastward-propagating Rossby waves. Around the end, the phase speed drops below average across the entire vertical column. Additionally, the phase speed stays below average after reflection events have ended and decreases in the stratosphere even further around +10 days, potentially indicating a weakening of the stratospheric circulation after reflection events. However, as Messori et al. (2022) noted, this weakening is not sufficient to cause a significant drop in zonal-mean zonal winds, but could rather be connected to a stretched stratospheric polar vortex, displaced towards Eurasia.

Anomalies in ISP confirm the change of Rossby wave behaviour during reflection events, but highlight differences in the vertical structure. The overall Rossby wave activity mostly remains close to its climatological average and only increases in the stratosphere after the end of reflection events (Fig. 6 b). However, when focusing on ISP_{west}, an increase in Rossby wave activity becomes discernible prior to the end of reflection events. This begins in the lower troposphere around day -9 and in the stratosphere only around day -4 (Fig. 6 c). The enhanced westward propagation of Rossby waves beginning in the lower troposphere coincides temporally with the previously-mentioned strong decrease of 2m air temperatures over North America and influences the upper levels only at a later stage. Positive anomalies of ISP_{east} align with periods of enhanced phase speed around the onset of reflection events (cf. Fig. 6 a and d). During the end of reflection events, ISP_{east} is suppressed in the lower troposphere, while Rossby waves are more active in the stratosphere.

To summarize, space-time spectral analysis highlights the enhancement of westward-propagating Rossby waves towards the end of reflection events. This is particularly pronounced in westward-propagating waves 1, 3 and 4, and coincides with

https://doi.org/10.5194/egusphere-2024-2240
Preprint. Discussion started: 30 July 2024

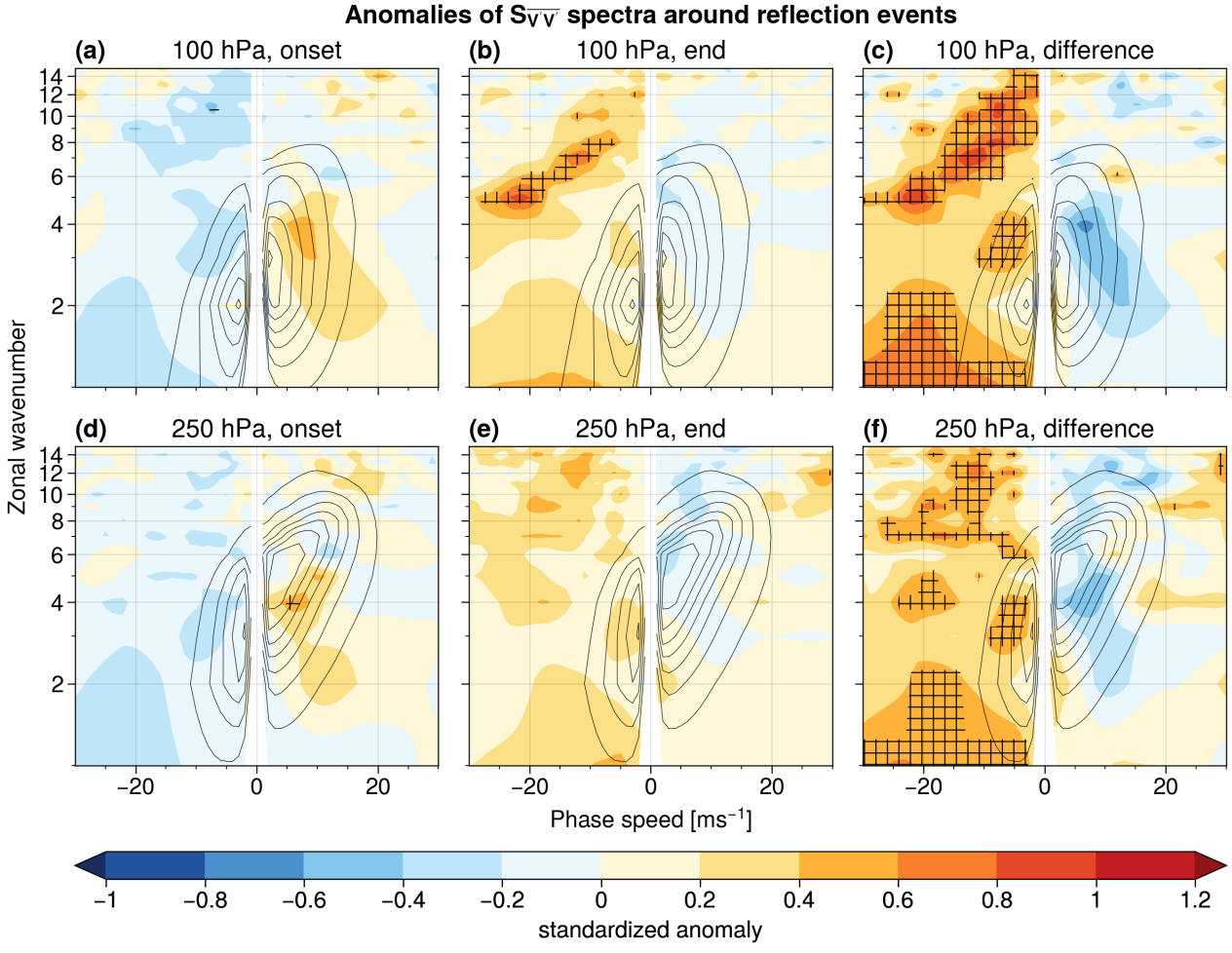

Figure 5. Standardized anomalies of spectral power $S_{\overline{v'v'}}$ of each harmonic at 100 hPa during (a) reflection event onset, (b) end and (c) difference between onset and end are represented in shading. Sub-panels (d) - (e) show the same, but for 250 hPa. Black contours show the DJFM mean for all years (100 hPa: steps of $0.05\,m^2\,s^{-2}\,\Delta c^{-1}$ from $0.05\,m^2\,s^{-2}\,\Delta c^{-1}$ to $0.35\,m^2\,s^{-2}\,\Delta c^{-1}$; 250 hPa: steps of $0.1\,m^2\,s^{-2}\,\Delta c^{-1}$ from $0.1\,m^2\,s^{-2}\,\Delta c^{-1}$ to $0.7\,m^2\,s^{-2}\,\Delta c^{-1}$). Horizontal hatching indicates significant negative anomalies, cross-hatching indicates significant positive anomalies.

a lower phase speed than normal. Westward-propagating Rossby waves become more active at first in the lower troposphere, approximately 9 days before the end of reflection events, and then in the stratosphere a few days later.

https://doi.org/10.5194/egusphere-2024-2240
Preprint. Discussion started: 30 July 2024

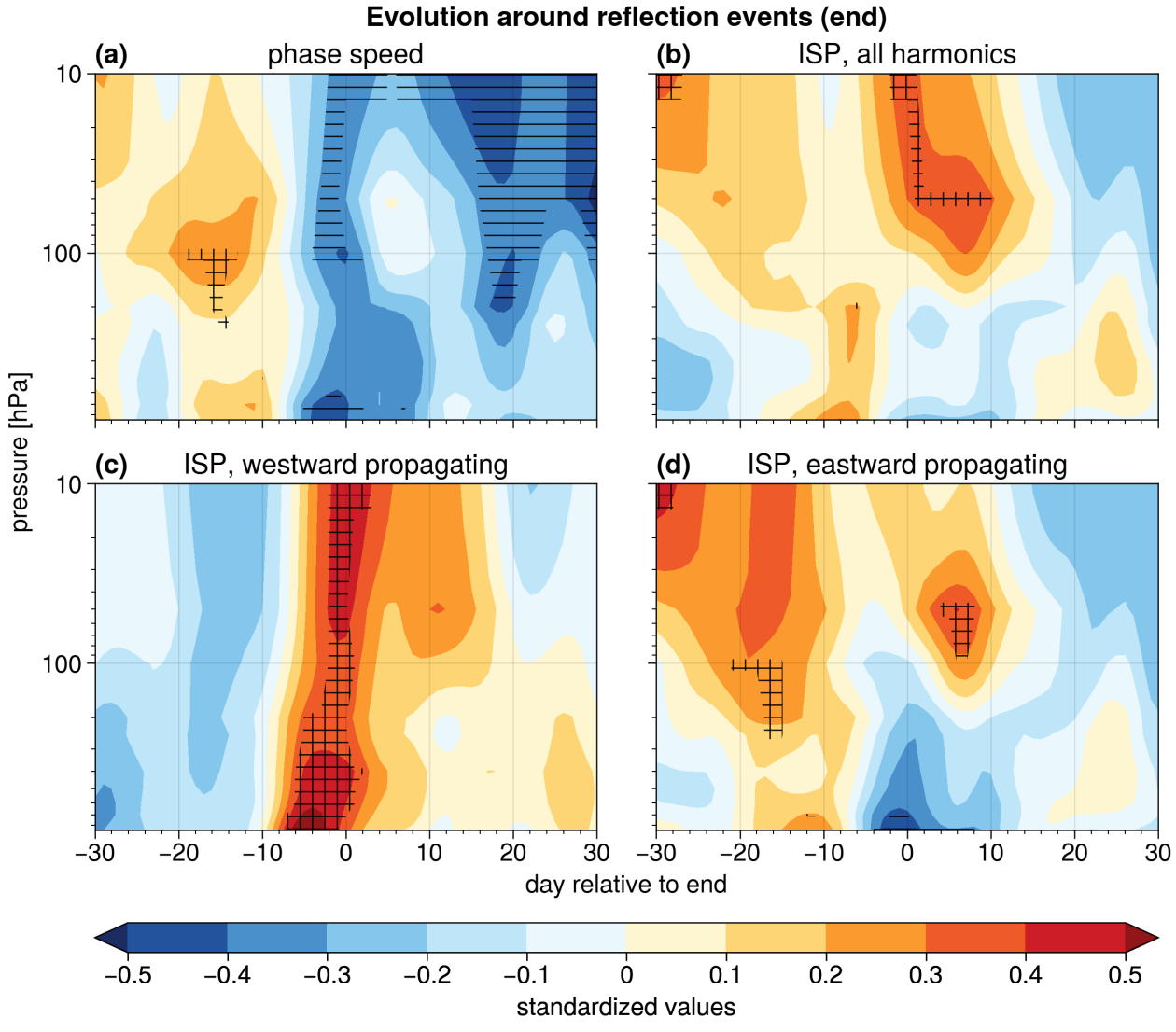

Figure 6. Vertical cross-section of standardized anomalies of (a) phase speed, (b) ISP, (c) ISP_{west} and (d) ISP_{east} derived from spectral power $\mathrm{S}_{\overline{\mathrm{V}'\mathrm{V}'}}$ between 850 hPa and 10 hPa centered around the end date of reflection events. Horizontal hatching marks significant negative anomalies, cross-hatching significant positive anomalies.

https://doi.org/10.5194/egusphere-2024-2240
Preprint. Discussion started: 30 July 2024

3.2 Connecting reflection events to tropospheric weather regime evolution

Messori et al. (2022) attested an association between reflection events and transitions from the Pacific Trough (PT) to the Alaskan Ridge (AKR) weather regime. Given that the spatial patterns shown in Section 3.1.2 are consistent with this transition, we now discuss the characteristics of the regime shift and its similarity to reflection events.

During transitions from PT to AKR, the signal in geopotential height anomalies extends from the stratosphere to the lower troposphere, with a clear barotropic character similar to that during reflection events (Fig. 7 a–c). The transition begins about 12 days before the central date of AKR with a negative geopotential height anomaly centered at approximately 140 °W, i.e., the circulation anomaly characteristic of the PT. This is followed by a positive geopotential height anomaly, i.e. the AKR, which replaces the PT. Both anomalies propagate westward, as observed during reflection events (cf. Figs. 3 and 7). In parallel, a new negative anomaly downstream of the ridge forms at approximately 80°W during the AKR regime, and persists for some time afterwards (Fig. 7 a–c). The geopotential anomalies are most pronounced in the mid-upper troposphere, in part likely due to the regimes being defined at 500 hPa (Lee et al., 2023a). Anomalies in WAF behave similarly during the regime transition compared to reflection events, with the only differences being a stronger eastward component at higher levels and a more pronounced upward WAF at 850 hPa during PT–AKR transitions.

During the regime transition from PT to AKR, the evolution of ISP_{west} anomalies is comparable to that during reflection events. In agreement with the westward propagation of the ridge, ISP_{west} takes anomalously weak values during the PT regime and stronger-than-average values during AKR, evidencing a change in the Rossby wave behaviour resembling that between onset and end of reflection events (cf. Figs. 3 d and 7 d).

Changes in the Rossby wave spectrum from PT to AKR are also in agreement with those observed during reflection events, except for the lack of significant differences for wave-1. The difference between the AKR and PT spectra highlights the enhancement of spectral power for westward-propagating waves-3 and 4. Additional significant anomalies occur in phase-space regions with low spectral power (Fig. 8 a, b, d, e). This agrees with the change of Rossby wave behaviour during reflection events (cf. Figs. 5 c, f and 8 c, f). As in the case of geopotential height anomalies, Rossby wave spectra anomalies of PT and AKR are more pronounced at 250 hPa than in the stratosphere (cf. Figs. 8 and A5).

In summary, the transition from a PT to an AKR weather regime resembles the atmospheric evolution during reflection events, confirming previous research (Messori et al., 2022). About one-third of the transition events occur during reflection events (21 out of 62). We also note that reflection events happening without PT around the onset, or without AKR around the end, show a weaker signal in tropospheric circulation (not shown). Our analysis further points to the enhancement of westward-propagating wave-3 and wave-4 during reflection events being related to the PT to AKR regime shift. In contrast, the lack of a signal in wave-1 in the spectra of weather regimes suggests that the latter signal arises from the stratosphere during reflection events (cf. Figs. 5 c, f and 8 c, f).

https://doi.org/10.5194/egusphere-2024-2240
Preprint. Discussion started: 30 July 2024

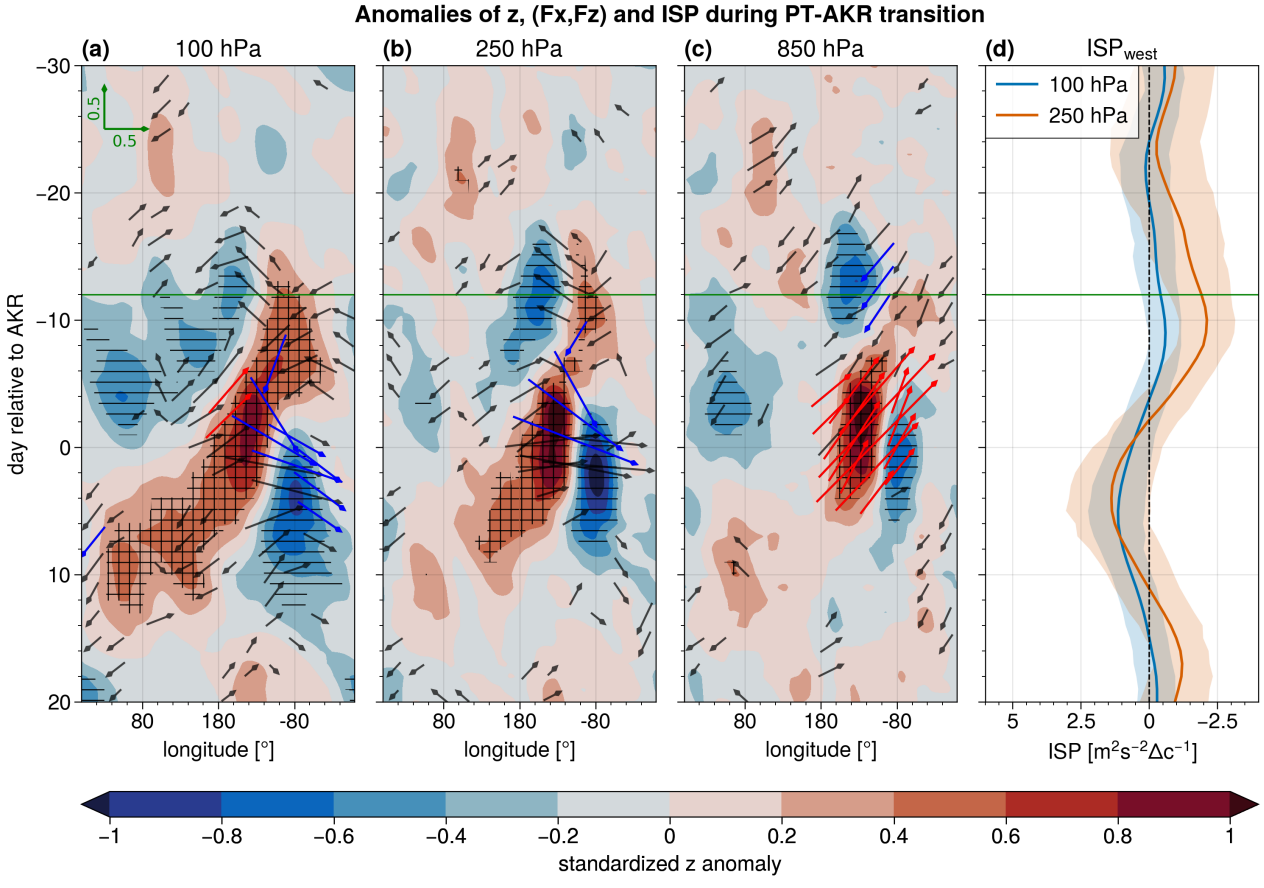

Figure 7. As in Fig. 3, but centred around the central date of AKR during PT–AKR transitions 2.2.

https://doi.org/10.5194/egusphere-2024-2240
Preprint. Discussion started: 30 July 2024

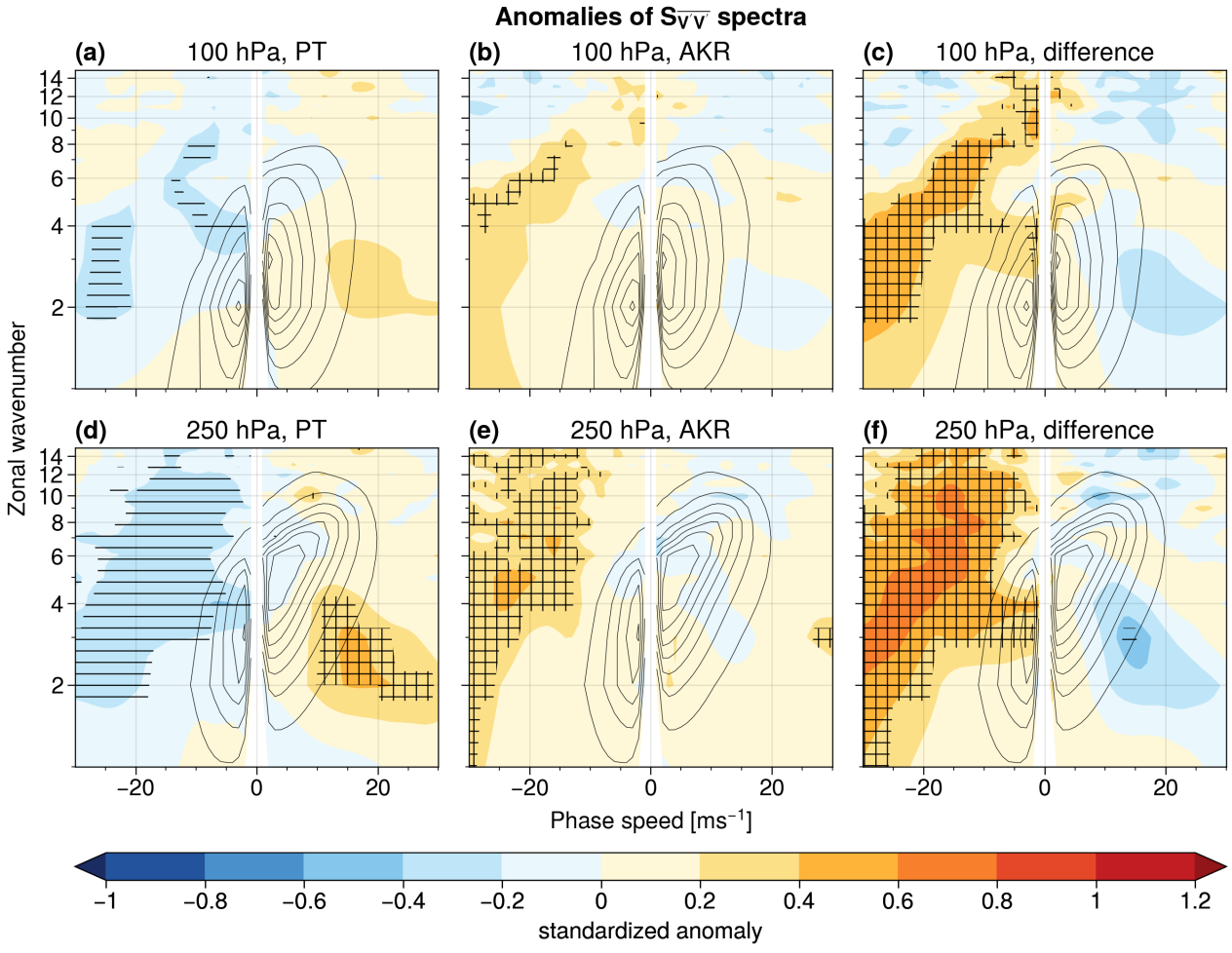

Figure 8. As Fig. 5, but for (a, d) PT regimes, (b, e) AKR regimes and (c, f) difference between PT and AKR regimes at 100 hPa and 250 hPa.

https://doi.org/10.5194/egusphere-2024-2240
Preprint. Discussion started: 30 July 2024

3.3 Signal regionalization

The preceding sections focus on the dynamics over the North Pacific, but also highlight the possible impact of reflection events on other regions of the Northern Hemisphere. In contrast to the reflection index, space-time wave spectra are computed over a full hemispheric domain, raising the question if the overall signal is dominated by reflection events or if unrelated Rossby waves contribute to the spectral signature. To address this, we evaluate the spectral properties of a new sample of "regionalized events", selected based on the correlation of the 100 hPa geopotential height field over the North Pacific with reflection events (section 2.2).

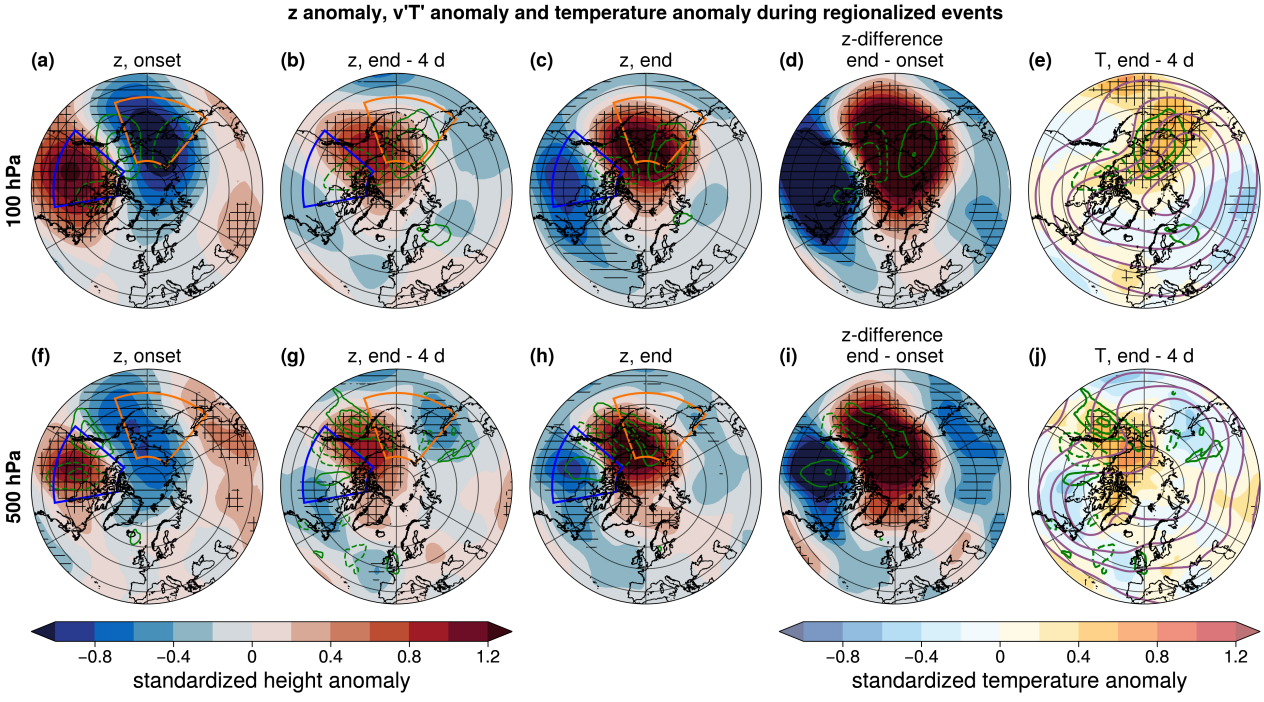

Figure 9. As Fig. 4, but for regionalized events (Sec. 2.2).

The geopotential height anomalies of the regionalized events composite exhibit (by definition) an alignment with those in reflection events in the Siberian and Canadian domains, albeit with larger amplitude (cf. Figs. 4 and 9). A second similarity with the reflection events consists in the westward propagation of the Canadian ridge (first three columns in Fig. 9). However, when comparing regionalized events with reflection events, there is a lower level of agreement over Eurasia. This is particularly evident for the difference between onset and end days (cf. Figs. 4 d, i and 4 d, i) and points to the uniqueness of reflection events and their connection to the hemispheric circulation. Despite the difference in geopotential height anomalies, 19 out of 63 regionalized onset events overlap with the onset of reflection events, and 17 of the 54 regionalized end events overlap with the end of reflection events. This overlap indicates that the definition of reflection events using $v'T'$ anomalies over the North Pacific corresponds to a relatively systematic pattern of geopotential height anomalies over that region. The regionalized events

https://doi.org/10.5194/egusphere-2024-2240
Preprint. Discussion started: 30 July 2024

show similar temperature anomalies to the reflection events, albeit with weaker anomalies in the stratosphere over Canada (cf. Figs. 4 e, j and 4 e, j).

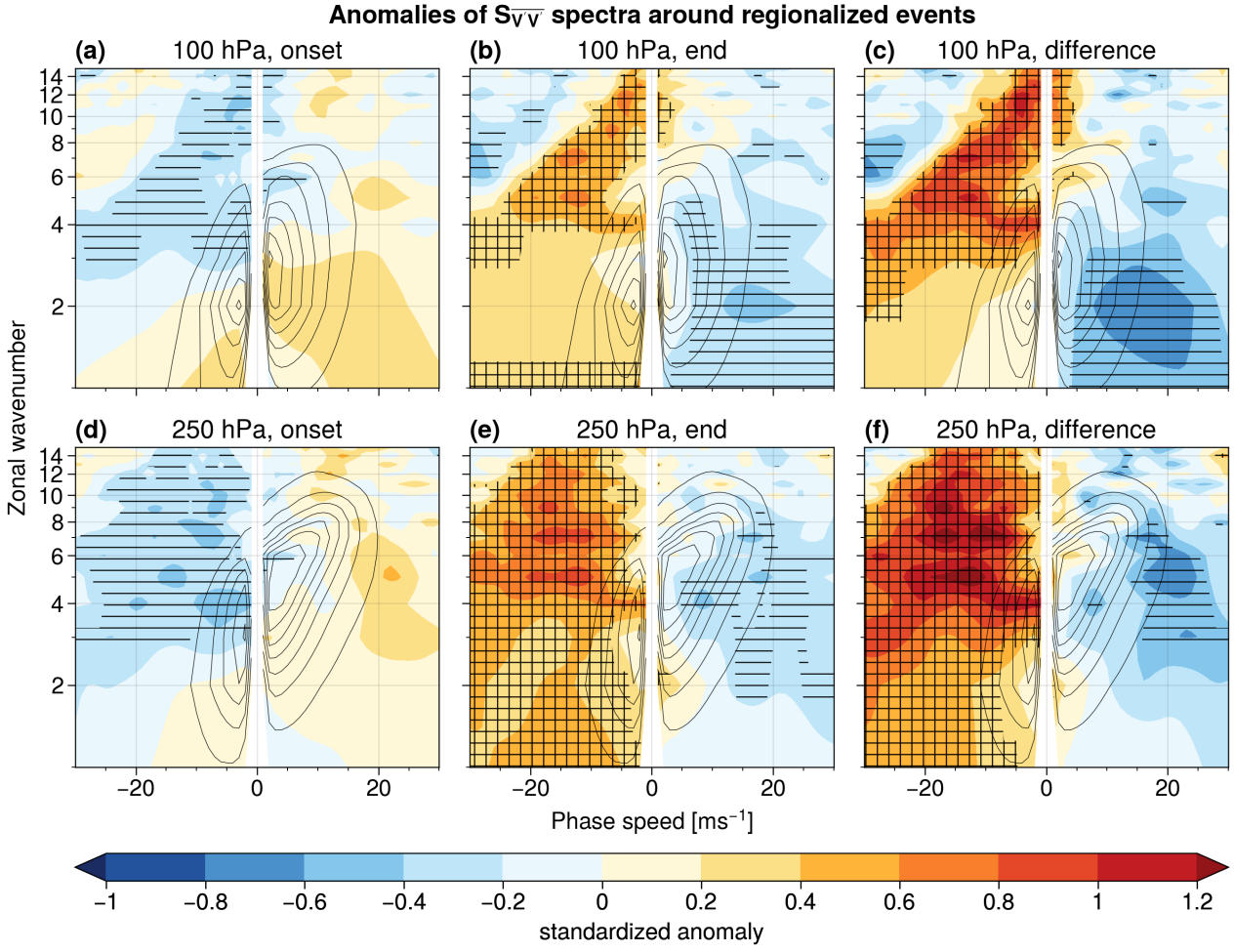

Figure 10. As Fig. 5, but for regionalized events (Sec. 2.2).

The signature in space-time spectra of regionalized events is similar to reflection events (cf. Figs. 5 and 10). During the regionalised onset events, eastward-propagating waves are more active with respect to climatology, while enhanced activity for westward propagating Rossby waves characterizes the end events. The lack of a significant difference between regionalized onset and end events in westward wave-1 at 100 hPa could arise from an already enhanced westward-propagating wave-1 during the onset time (Fig. 10 a and c). Nevertheless, the difference between regionalized onset and end events agrees in most other climatologically relevant phase-space regions with the difference between onset and end of reflection events, including wave-1 at 250 hPa (cf. Figs. 5 c, f and 10 c, f). Furthermore, the decrease of Rossby wave activity for eastward-propagating waves is more pronounced for regionalized events than for reflection events, yet over a similar range of wavenumbers.

https://doi.org/10.5194/egusphere-2024-2240
Preprint. Discussion started: 30 July 2024

To summarize, the shift to enhanced westward-propagating Rossby waves is similar both in regionalized events and reflection events. Even though geopotential height anomalies over Eurasia differ between these events, the key feature of a westward propagating ridge over the North Pacific is represented in regionalized events. The similar behaviour of Rossby wave space-time spectra in both types of events emphasizes the effectiveness of hemispheric space-time spectral analysis for quantifying changes of Rossby wave dynamics associated with North Pacific reflection events.

https://doi.org/10.5194/egusphere-2024-2240
Preprint. Discussion started: 30 July 2024

3.4 Impact on windiness over Europe

There is a growing literature connecting cold spells in North America to wet and/or windy extremes in Europe, sometimes termed pan-Atlantic extremes (Messori et al., 2016; Ding et al., 2022; Leeding et al., 2023a, b; Riboldi et al., 2023; Messori and Faranda, 2023). In our study, we confirm previous results showing that reflection events over the North Pacific are connected to a drop in temperatures over North America (Messori et al., 2022; Kodera et al., 2016; Kretschmer et al., 2018; Matthias and Kretschmer, 2020). Additionally, we highlight the presence of hemispheric-scale anomalies in the mid-latitude circulation. Based on these results and on the literature on pan-Atlantic extremes, we now investigate whether the reflection events correspond to 10m wind anomalies in Europe. Recently, Riboldi et al. (2023) highlighted two possible pathways connecting cold temperatures over North America and extreme wind events in Europe. The atmospheric evolution during reflection events resembles the first pathway. This involves the propagation of a Rossby wave train from the North Pacific resulting in an intensification of the North Atlantic eddy-driven jet and windy extremes over northwestern Europe a few days after the cold spell peak over North America.

As the coldest temperatures over North America typically occur a few days before the end of a reflection event (Messori et al., 2022; Millin et al., 2022), one would expect windy extremes over Europe around the end of reflection events. Confirming this expectation, one day after the end date there is a noticeable increase in average wind speeds across northwestern Europe, albeit only in the order of 1 ms^{-1} (Fig. 11 a and Fig. A6). Despite that, wind speeds exceed the local 98th percentile – often used to identify damaging wind extremes – two to five times more often than on average (Fig. 11 b). Consistent with the first pathway outlined by Riboldi et al. (2023), we also observe a strengthening of the jet stream over the North Atlantic, with the jet exit region over northwestern Europe (Fig. 11 c and Fig. A6).

This highlights a previously unreported connection between wind extremes in Europe and reflection events in the North Pacific. The jet stream anomalies that we find are in line with earlier findings about the connection between reflection events and atmospheric dynamics over the North Atlantic (Kodera et al., 2016) and with the impact on the tropospheric circulation of zonally-averaged hemispheric downward-propagating stratospheric wave events (Dunn-Sigouin and Shaw, 2015; Shaw et al., 2014; Shaw and Perlwitz, 2013).

https://doi.org/10.5194/egusphere-2024-2240
Preprint. Discussion started: 30 July 2024

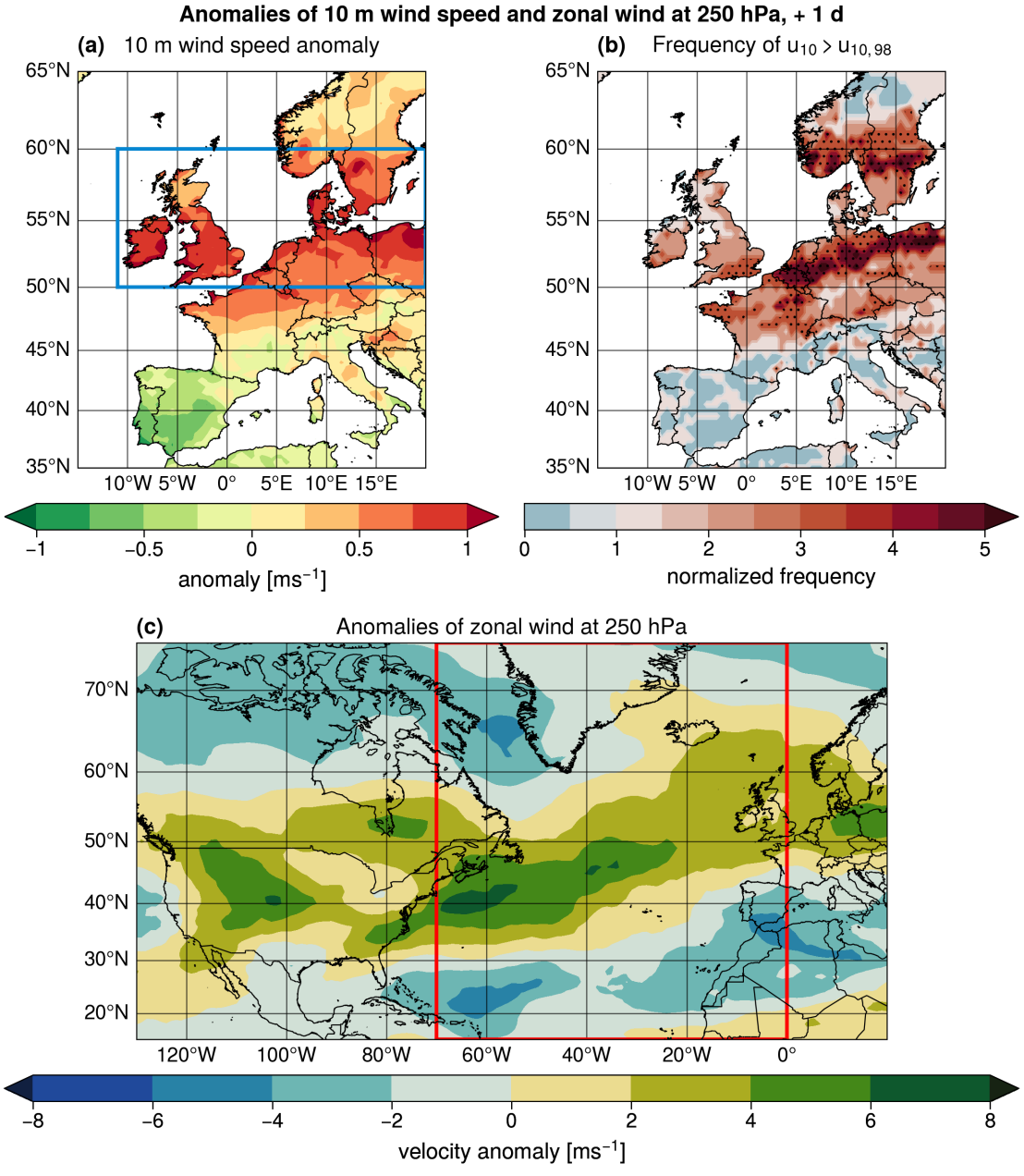

Figure 11. (a) Composite 10-m wind speed anomaly in Europe one day after the end of the reflection events. (b) Frequency of 10-m wind speed exceeding the local 98th percentile at each grid point, normalized with respect to the climatological frequency of 2% ($\geq$ 1: above average, $\leq$ 1: below average). (c) 250 hPa zonal wind anomalies. Stippling in (b) indicates regions where the 98th percentile of 10-m wind speed is exceeded at least 2.5 times more often than the DJFM average. The blue box in (a) and the red box in (c) indicate the regions used to calculate the mean 10-meter wind and jet strength, respectively, shown in Fig. A6.

https://doi.org/10.5194/egusphere-2024-2240
Preprint. Discussion started: 30 July 2024

4 Discussion and conclusions

Stratospheric wave reflection events, identified by anomalies in meridional eddy heat flux $v'T'$ at 100 hPa across the North Pacific, show a distinct vertical structure. Most of the significant $v'T'$ anomalies are located in the stratosphere and show a pattern alternating in sign before the onset and after the end of the reflection events. This is connected to the westward propagation of a ridge from Canada to Siberia and beyond, resembling a shift from a Pacific Trough (PT) – type circulation to an Alaskan Ridge (AKR). Space-time spectral analysis of Rossby waves indicates an increased activity in westward-propagating waves, which is similar between reflection events and regime transitions from PT to AKR. However, a stronger stratospheric signal is found during reflection events. Since the Rossby wave spectra are based on hemispheric data, we implement a regionalised analysis to confirm that the signals displayed in the spectra originate chiefly from dynamics linked to the reflection events. We further find that the reflection events correspond to a temperature decrease over North America, as noted in earlier research, but we also connect them for the first time to anomalously frequent wind extremes over Europe.

A key result of our analysis is the accelerating westward propagation of Rossby waves during reflection events. This may be explained by the slowdown of the circulation due to Rossby wave absorption in the stratosphere. Following the period of wave reflection over the North Pacific, upward propagating Rossby waves from the northwest Pacific could eventually be absorbed, disrupting and weakening the stratospheric polar vortex (Matsuno, 1971; Sjoberg and Birner, 2012; Polvani and Waugh, 2004; Reichler and Jucker, 2022). This is supported by the weak correspondence between SSWs and reflection events reported by Messori et al. (2022). Furthermore, the anomalously strong planetary Rossby waves in the stratosphere are in line with the observed stretching of the stratospheric polar vortex connected to reflection events (Messori et al., 2022; Cohen et al., 2022). As a result of the changed circulation, the strengthened Alaskan Ridge that characterizes reflection events propagates westward. This weakens the positive $v'T'$ anomalies over the Siberian domain and ends the reflection events.

While wave amplification over Eurasia can trigger reflection events over the North Pacific (Cohen et al., 2022), the tropical Pacific could also play a role due to its link with blocking at higher latitudes (e.g., Renwick and Wallace, 1996; Henderson and Maloney, 2018; Carrera et al., 2004). Indeed, previous work has connected blocking patterns and stratospheric wave reflections over the North Pacific, highlighting their role in modulating 2-m air-temperature over North America (Guan et al., 2020; Kodera et al., 2013; Millin et al., 2022). In this context, the activity of wave-1 plays a crucial role (Ding et al., 2022; Kodera et al., 2016) by contributing to troposphere-stratosphere coupling (Dunn-Sigouin and Shaw, 2015; Shaw and Perlwitz, 2013). This agrees with our analysis highlighting the additional role of wave-1 during stratospheric reflection events, while we attest changes in wave-3 and 4 to a transition of tropospheric weather regimes. Complementary to the role of wave-1, a vertical maximum of zonal winds in the middle stratosphere is suggested to be a necessary precondition for stratospheric wave reflection (Perlwitz and Harnik, 2004; Messori et al., 2022). Given the enhancement of westward-propagating Rossby waves during reflection events, there could also exist a connection to occurrences of retrograding waves (Branstator, 1987; Kushnir, 1987; Madden and Speth, 1989; Raghunathan and Huang, 2019), or to the recently-defined 'Stratosphere-Troposphere Oscillation' (Shen et al., 2023). These open questions point to future research pathways for deepening our understanding of the tropospheric mechanisms driving wave reflection events over the North Pacific and their connection to other modes of stratosphere-troposphere coupling.

https://doi.org/10.5194/egusphere-2024-2240
Preprint. Discussion started: 30 July 2024

Although the exact mechanisms driving the end or onset of stratospheric reflection events over the North Pacific remain to be unravelled, our study has highlighted a systematic dynamical evolution during these events. We have further found a possible connection between reflection events and European wind extremes. Both this and the previously noted temperature drop over North America could provide valuable information for extended-range prediction.

https://doi.org/10.5194/egusphere-2024-2240
Preprint. Discussion started: 30 July 2024

Appendix A: Additional Figures

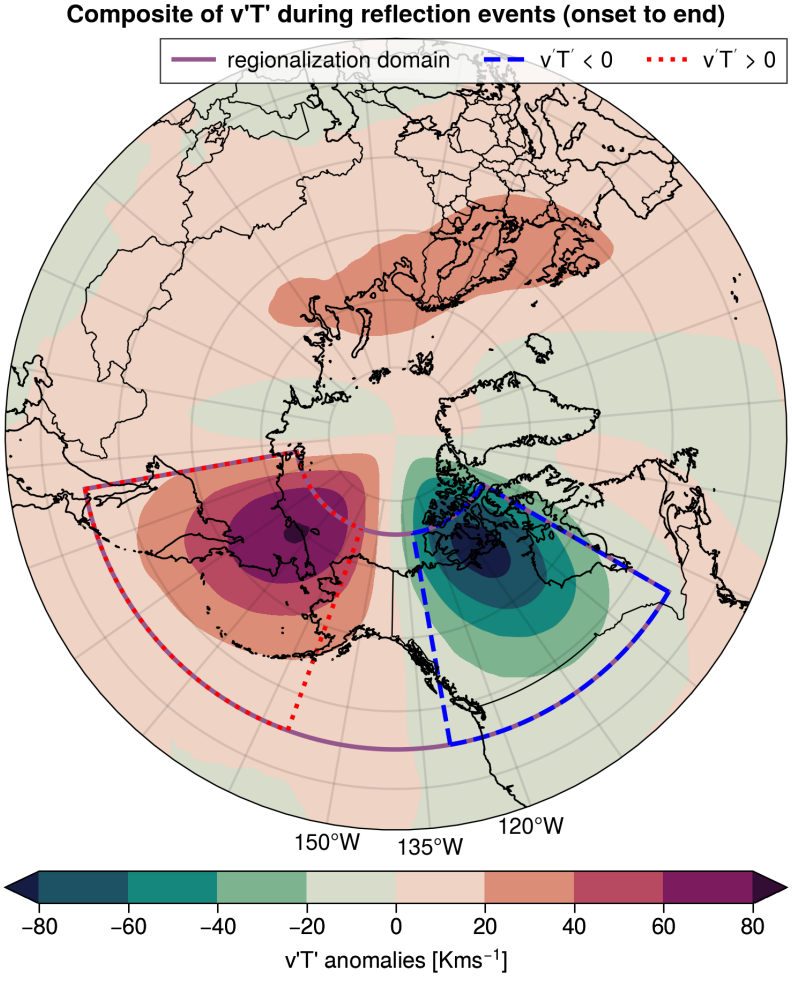

Figure A1. Contours: composite of $v'T'$ anomalies during all days of reflection events from their onset until the end; boxes: location of (red, dotted) the Siberian domain located between 45-75°N, 140-200°E, (blue, lined) Canadian domain located between 45-75°N, 230-280°E, used to define reflection events and (purple) the domain used to obtain regionalized events (Section 2.2).

https://doi.org/10.5194/egusphere-2024-2240
Preprint. Discussion started: 30 July 2024

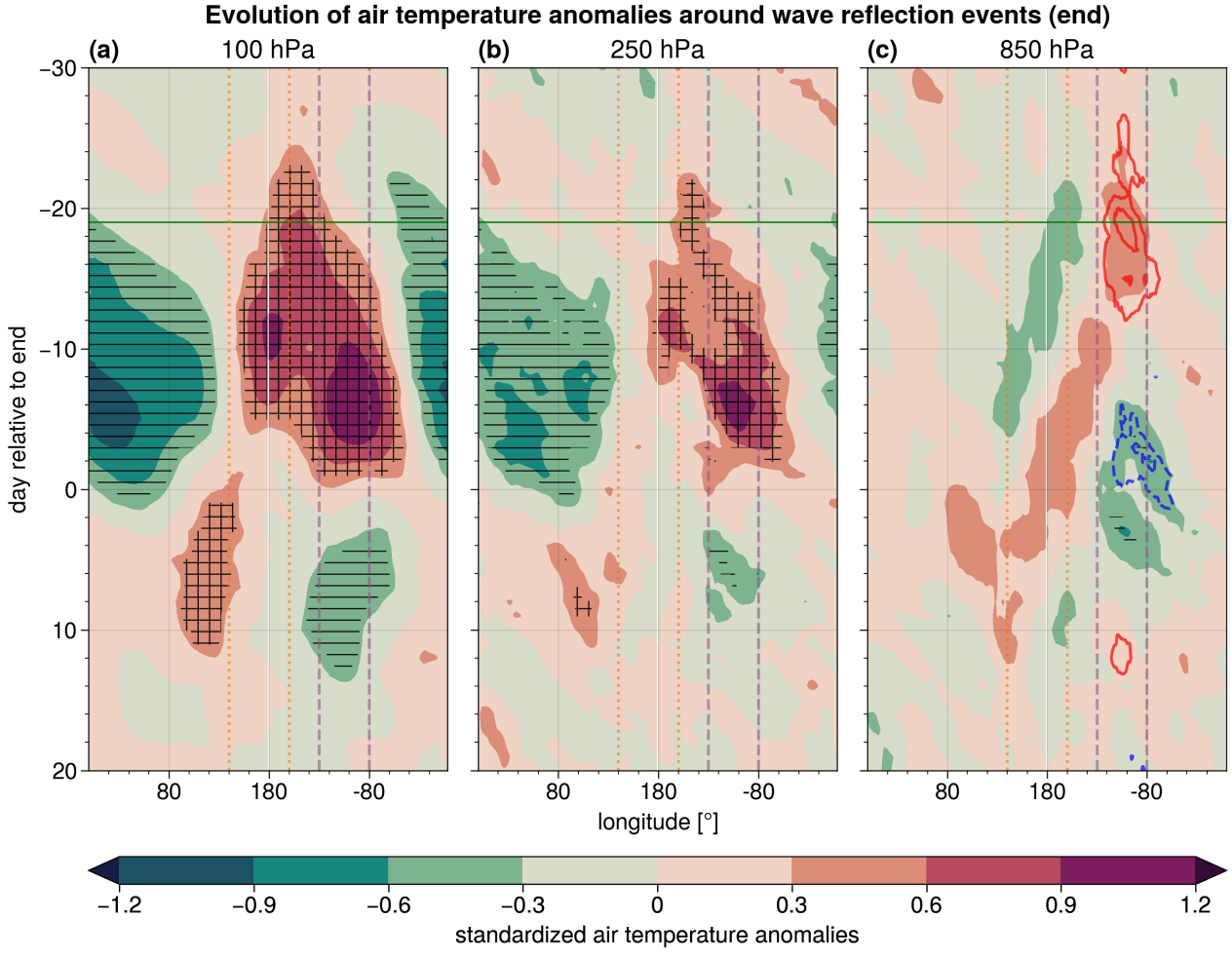

Figure A2. As Fig. 2, but for air temperature at (a) 100 hPa, (b) 250 hPa and (c) 850 hPa.

https://doi.org/10.5194/egusphere-2024-2240
Preprint. Discussion started: 30 July 2024

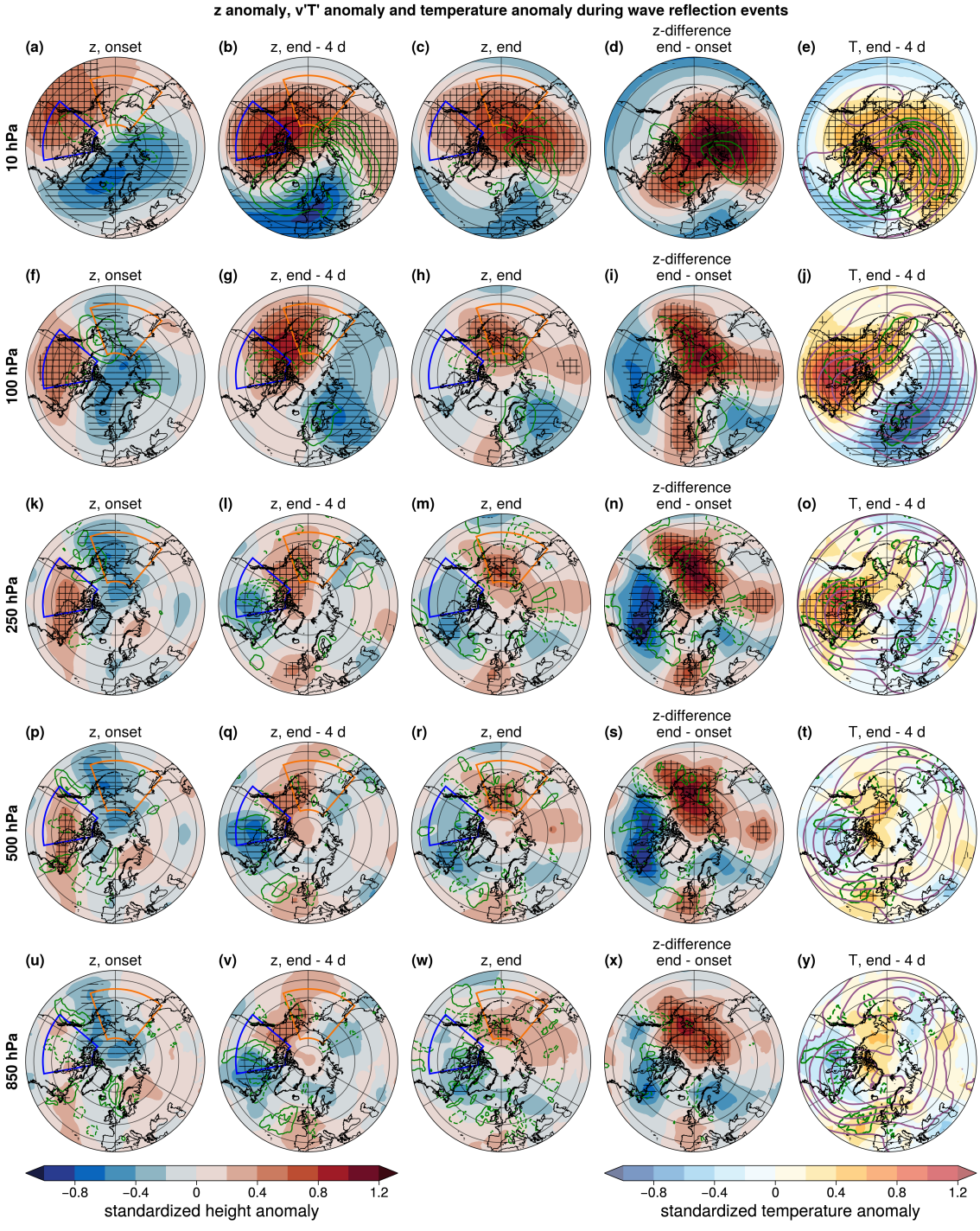

Figure A3. As Fig. 4, but for pressure levels 10 hPa, 100 hPa, 250 hPa, 500 hPa and 850 hPa.

https://doi.org/10.5194/egusphere-2024-2240
Preprint. Discussion started: 30 July 2024

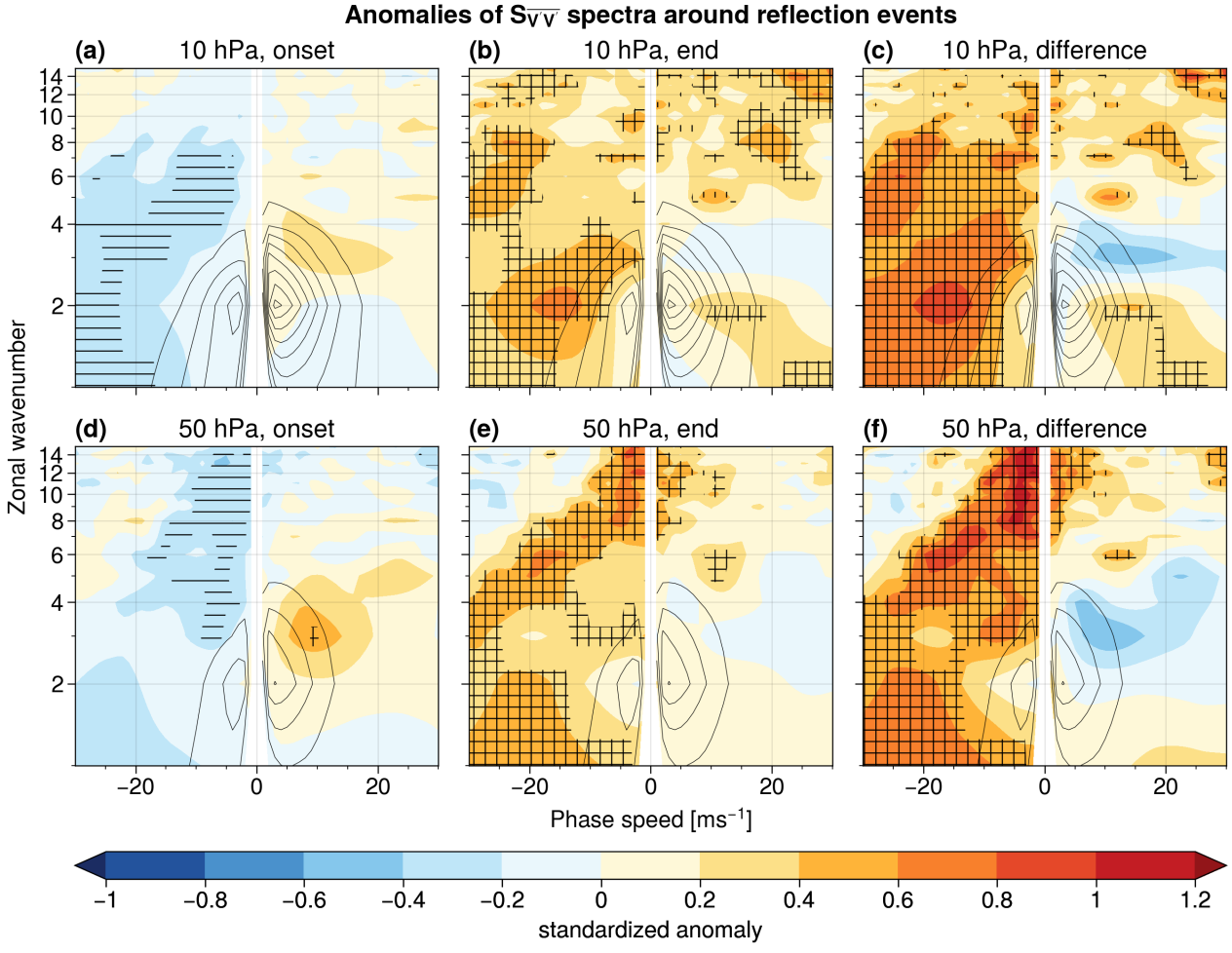

Figure A4. As Fig. 5, but for pressure levels 10 hPa and 50 hPa.

https://doi.org/10.5194/egusphere-2024-2240
Preprint. Discussion started: 30 July 2024

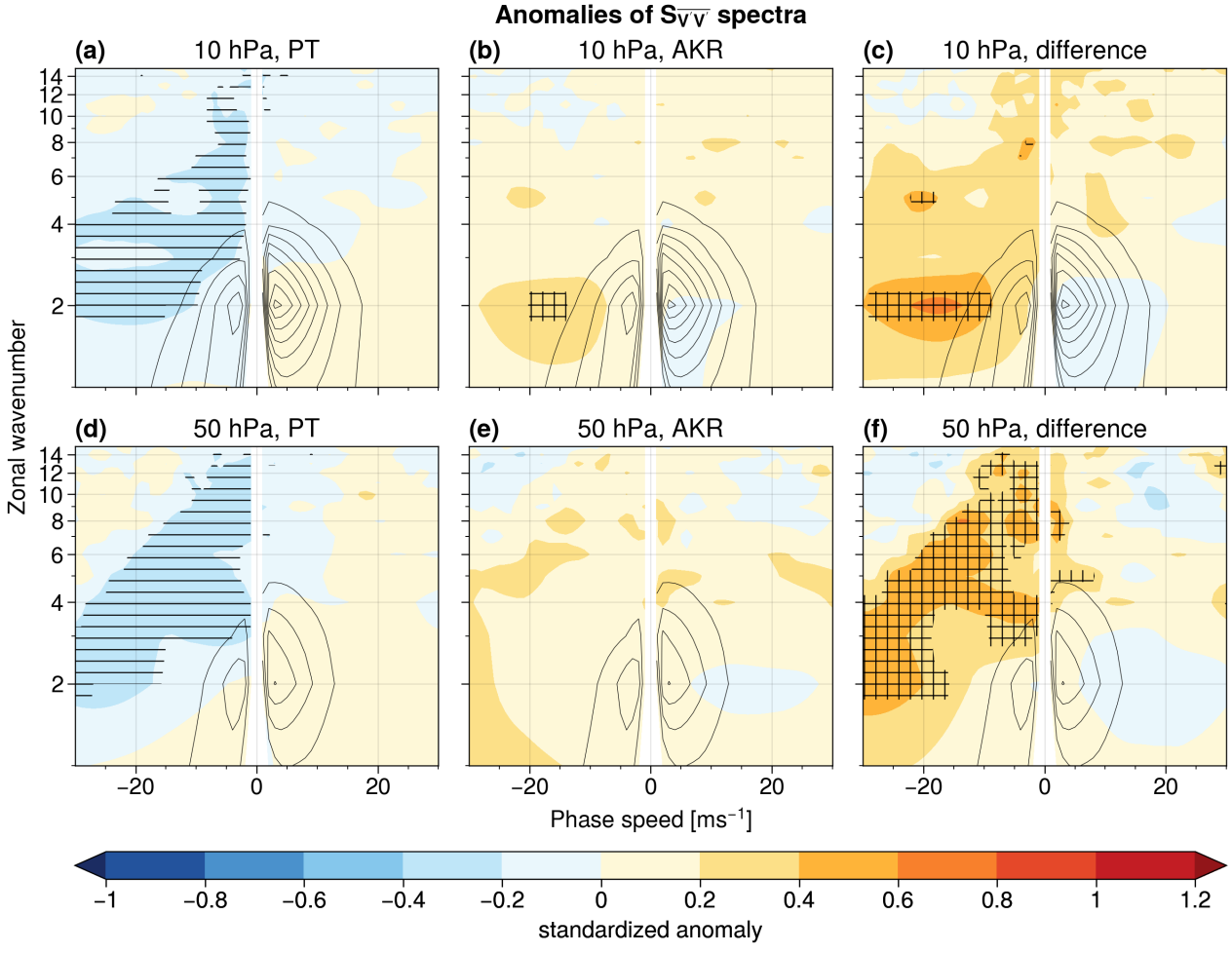

Figure A5. As Fig. 5, but for (a, d) PT regimes, (b, e) AKR regimes and (c, f) difference between PT and AKR regimes at 10 hPa and 50 hPa.

https://doi.org/10.5194/egusphere-2024-2240
Preprint. Discussion started: 30 July 2024

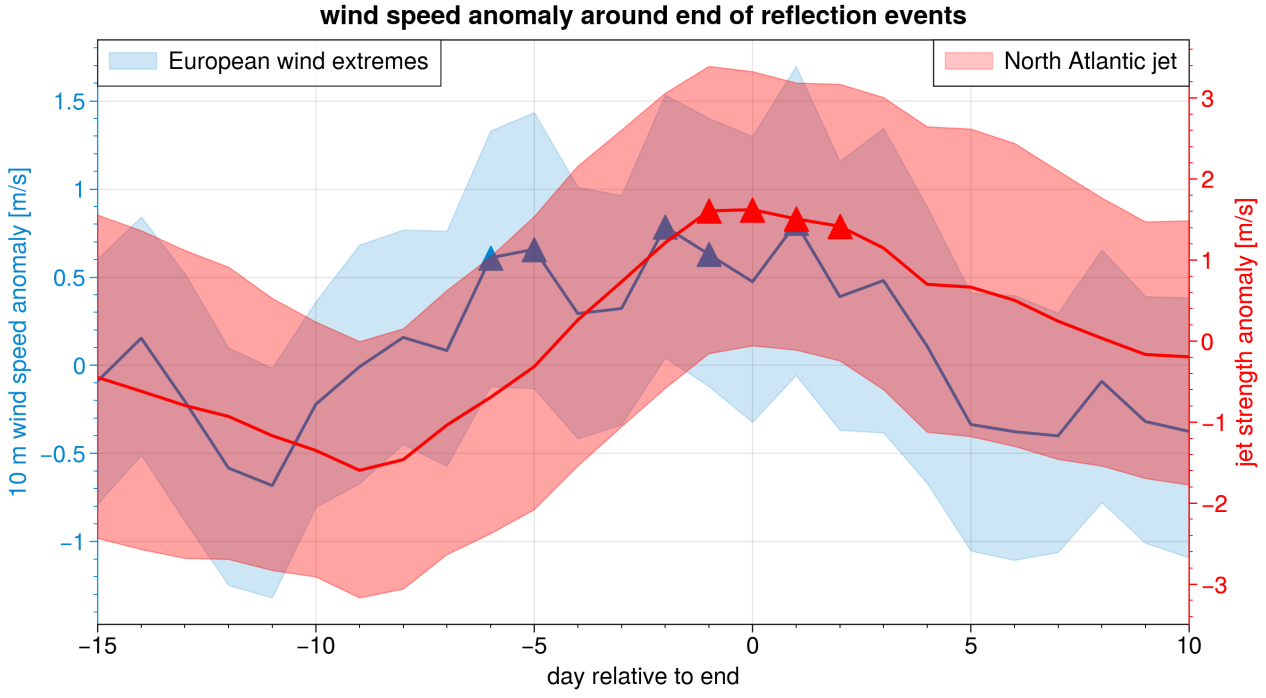

Figure A6. Anomaly of cosine-latitude weighted mean of 10-m wind speed over land grid points of Northern Europe (50-60°N, 11°W-20°E; blue box in Fig. 11 a) and anomaly of the jet strength. The jet strength is computed similarly to Woollings et al. (2010), but adapted to our study: The zonal average of the 250 hPa zonal wind over the North Atlantic (15-75°N, 70-0°W; red box in Fig. 11 c) is smoothed with a centered 10-day running mean at each latitude. Subsequently the maximum wind speed is identified to define the jet strength on a given day which is then deseasonalized following Sec. 2.1. Shading indicates the 95% confidence interval of the mean and triangles highlight dates where the composite anomaly is above the 95th percentile of a resampled distribution of 10 000 means of 45 randomly selected days from the climatology.

https://doi.org/10.5194/egusphere-2024-2240
Preprint. Discussion started: 30 July 2024

Code and data availability. The ERA5 data used to compute the reflection events and the wave spectra is freely available from https://doi.org/10.24381/cds.bd0915c6 (Hersbach et al., 2024) The code for the wave spectra is available from the authors upon request. An example data set of space-time spectra of Rossby waves at 10 hPa and 250 hPa is available at https://snd.se/en/catalogue/dataset/preview/440eef3a-c462-458a-bdf1-b83e8c10b4f3/1 (Riboldi and Schutte, 2024).

Author contributions. MS and GM designed the analysis. MS analyzed the data and prepared the figures with feedback from GM, AP and SL. MS drafted the first version of the manuscript in collaboration with all co-authors.

Competing interests. The authors declare that they have no conflict of interest.

Acknowledgements. We thank Jacopo Riboldi for computing the space-time spectra of Rossby waves. MS thanks Meriem Krouma, Iana Strigunova, Richard Leeding and Leonardo Olivetti for valuable input resulting from discussions about the results. MS and GM acknowledge funding from the European Research Council (ERC) under the European Union's Horizon 2020 research and innovation program (grant agreement no. 948309, CENÆ project). AP is funded from the Swiss National Science Foundation (SNF) Grant Number IZCOZ0_205461.

https://doi.org/10.5194/egusphere-2024-2240
Preprint. Discussion started: 30 July 2024

References

Afargan-Gerstman, H., Polkova, I., Papritz, L., Ruggieri, P., King, M. P., Athanasiadis, P. J., Baehr, J., and Domeisen, D. I. V.: Stratospheric influence on North Atlantic marine cold air outbreaks following sudden stratospheric warming events, Weather Clim. Dynam., 1, 541–553, https://doi.org/10.5194/wcd-1-541-2020, 2020.

Albers, J. R. and Birner, T.: Vortex Preconditioning due to Planetary and Gravity Waves prior to Sudden Stratospheric Warmings, J. Atmos. Sci., 71, 4028 – 4054, https://doi.org/10.1175/JAS-D-14-0026.1, 2014.

Baldwin, M. P. and Dunkerton, T. J.: Stratospheric Harbingers of Anomalous Weather Regimes, Science, 294, 581–584, https://doi.org/10.1126/science.1063315, 2001.

Birner, T. and Albers, J. R.: Sudden Stratospheric Warmings and Anomalous Upward Wave Activity Flux, SOLA, 13A, 8–12, https://doi.org/10.2151/sola.13A-002, 2017.

Branstator, G.: A Striking Example of the Atmosphere's Leading Traveling Pattern, J. Atmos. Sci., 44, 2310 – 2323, https://doi.org/10.1175/1520-0469(1987)044<2310:ASEOTA>2.0.CO;2, 1987.

Carrera, M. L., Higgins, R. W., and Kousky, V. E.: Downstream Weather Impacts Associated with Atmospheric Blocking over the Northeast Pacific, J. Climate, 17, 4823 – 4839, https://doi.org/10.1175/JCLI-3237.1, 2004.

Charlton, A. J. and Polvani, L. M.: A New Look at Stratospheric Sudden Warmings. Part I: Climatology and Modeling Benchmarks, J. Climate, 20, 449–469, https://doi.org/10.1175/JCLI3996.1, 2007.

Charlton-Perez, A. J., Ferranti, L., and Lee, R. W.: The influence of the stratospheric state on North Atlantic weather regimes, Q. J. Roy. Meteor. Soc., 144, 1140–1151, https://doi.org/10.1002/qj.3280, 2018.

Cohen, J., Barlow, M., Kushner, P. J., and Saito, K.: Stratosphere–Troposphere Coupling and Links with Eurasian Land Surface Variability, J. Climate, 20, 5335 – 5343, https://doi.org/10.1175/2007JCLI1725.1, 2007.

Cohen, J., Agel, L., Barlow, M., Furtado, J. C., Kretschmer, M., and Wendt, V.: The "Polar Vortex" Winter of 2013/2014, J. Geophy. Res. Atmospheres, 127, e2022JD036 493, https://doi.org/10.1029/2022JD036493, 2022.

de la Cámara, A., Birner, T., and Albers, J. R.: Are Sudden Stratospheric Warmings Preceded by Anomalous Tropospheric Wave Activity?, J. Climate, 32, 7173 – 7189, https://doi.org/10.1175/JCLI-D-19-0269.1, 2019.

Dell'Aquila, A., Lucarini, V., Ruti, P. M., and Calmanti, S.: Hayashi spectra of the northern hemisphere mid-latitude atmospheric variability in the NCEP–NCAR and ECMWF reanalyses, Clim. Dynam., 25, 639–652, https://doi.org/10.1007/s00382-005-0048-x, 2005.

Ding, X., Chen, G., Sun, L., and Zhang, P.: Distinct North American Cooling Signatures Following the Zonally Symmetric and Asymmetric Modes of Winter Stratospheric Variability, Geophys. Res. Lett., 49, e2021GL096 076, https://doi.org/10.1029/2021GL096076, 2022.

Domeisen, D. I. V. and Butler, A. H.: Stratospheric drivers of extreme events at the Earth's surface, Commun. Earth Environ., 1, e2019JD030 923, https://doi.org/10.1038/s43247-020-00060-z, 2020.

Domeisen, D. I. V., Grams, C. M., and Papritz, L.: The role of North Atlantic–European weather regimes in the surface impact of sudden stratospheric warming events, Weather. Clim. Dynam., 1, 373–388, https://doi.org/10.5194/wcd-1-373-2020, 2020.

Dunn-Sigouin, E. and Shaw, T. A.: Comparing and contrasting extreme stratospheric events, including their coupling to the tropospheric circulation, J. Geophys. Res. Atmospheres, 120, 1374–1390, https://doi.org/10.1002/2014JD022116, 2015.

Guan, W., Jiang, X., Ren, X., Chen, G., Lin, P., and Lin, H.: The Leading Intraseasonal Variability Mode of Wintertime Surface Air Temperature over the North American Sector, J. Climate, 33, 9287 – 9306, https://doi.org/10.1175/JCLI-D-20-0096.1, 2020.

https://doi.org/10.5194/egusphere-2024-2240
Preprint. Discussion started: 30 July 2024

Hall, R. J., Mitchell, D. M., Seviour, W. J. M., and Wright, C. J.: Tracking the Stratosphere-to-Surface Impact of Sudden Stratospheric Warmings, J. Geophys. Res.-Atmos., 126, e2020JD033 881, https://doi.org/10.1029/2020JD033881, 2021.

Hall, R. J., Mitchell, D. M., Seviour, W. J. M., and Wright, C. J.: Surface hazards in North-west Europe following sudden stratospheric warming events, Environ. Res. Lett., 18, 064 002, https://doi.org/10.1088/1748-9326/acd0c3, 2023.

Harnik, N.: Observed stratospheric downward reflection and its relation to upward pulses of wave activity, J. Geophys. Res. Atmospheres, 114, https://doi.org/10.1029/2008JD010493, 2009.

Harnik, N. and Lindzen, R. S.: The Effect of Reflecting Surfaces on the Vertical Structure and Variability of Stratospheric Planetary Waves, J. Atmos. Sci., 58, https://doi.org/10.1175/1520-0469(2001)058<2872:TEORSO>2.0.CO;2, 2001.

Henderson, S. A. and Maloney, E. D.: The Impact of the Madden–Julian Oscillation on High-Latitude Winter Blocking during El Niño–Southern Oscillation Events, J. Climate, 31, 5293 – 5318, https://doi.org/10.1175/JCLI-D-17-0721.1, 2018.

Hersbach, H., Bell, B., Berrisford, P., Hirahara, S., Horányi, A., Muñoz-Sabater, J., Nicolas, J., Peubey, C., Radu, R., Schepers, D., Simmons, A., Soci, C., Abdalla, S., Abellan, X., Balsamo, G., Bechtold, P., Biavati, G., Bidlot, J., Bonavita, M., De Chiara, G., Dahlgren, P., Dee, D., Diamantakis, M., Dragani, R., Flemming, J., Forbes, R., Fuentes, M., Geer, A., Haimberger, L., Healy, S., Hogan, R. J., Hólm, E., Janisková, M., Keeley, S., Laloyaux, P., Lopez, P., Lupu, C., Radnoti, G., de Rosnay, P., Rozum, I., Vamborg, F., Villaume, S., and Thépaut, J.-N.: The ERA5 global reanalysis, Q. J. Roy. Meteor. Soc., 146, 1999–2049, https://doi.org/10.1002/qj.3803, 2020.

Hersbach, H., Bell, B., Berrisford, P., Biavati, G., Horányi, A., Muñoz Sabater, J., Nicolas, J., Peubey, C., Radu, R., Rozum, I., Schepers, D., Simmons, A., Soci, C., Dee, D., and Thépaut, J.-N.: ERA5 hourly data on pressure levels from 1940 to present [data set], https://doi.org/10.24381/cds.bd0915c6, 2024.

Hitchcock, P. and Simpson, I. R.: The Downward Influence of Stratospheric Sudden Warmings, J. Atmos. Sci., 71, 3856 – 3876, https://doi.org/10.1175/JAS-D-14-0012.1, 2014.

Kidston, J., Scaife, A. A., Hardiman, S. C., Mitchell, D. M., Butchart, N., Baldwin, M. P., and Gray, L. J.: Stratospheric influence on tropospheric jet streams, storm tracks and surface weather, Nat. Geosci., 8, 433–440, https://doi.org/10.1038/ngeo2424, 2015.

Kodera, K., Mukougawa, H., and Itoh, S.: Tropospheric impact of reflected planetary waves from the stratosphere, Geophys. Res. Lett., 35, https://doi.org/10.1029/2008GL034575, 2008.

Kodera, K., Mukougawa, H., and Fujii, A.: Influence of the vertical and zonal propagation of stratospheric planetary waves on tropospheric blockings, J. Geophys. Res. Atmospheres, 118, 8333–8345, https://doi.org/10.1002/jgrd.50650, 2013.

Kodera, K., Mukougawa, H., Maury, P., Ueda, M., and Claud, C.: Absorbing and reflecting sudden stratospheric warming events and their relationship with tropospheric circulation, Journal of Geophysical Research: Atmospheres, 121, 80–94, https://doi.org/10.1002/2015JD023359, 2016.

Kolstad, E. W., Lee, S. H., Butler, A. H., Domeisen, D. I. V., and Wulff, C. O.: Diverse Surface Signatures of Stratospheric Polar Vortex Anomalies, J. Geophys. Res. Atmospheres, 127, e2022JD037 422, https://doi.org/10.1029/2022JD037422, 2022.

Kretschmer, M., Cohen, J., Matthias, V., Runge, J., and Coumou, D.: The different stratospheric influence on cold-extremes in Eurasia and North America, npj Clim. Atmos. Sci., 1, 44, https://doi.org/10.1038/s41612-018-0054-4, 2018.

Kushnir, Y.: Retrograding Wintertime Low-Frequency Disturbances over the North Pacific Ocean, J. Atmos. Sci., 44, 2727 – 2742, https://doi.org/10.1175/1520-0469(1987)044<2727:RWLFDO>2.0.CO;2, 1987.

Lee, S. H., Charlton-Perez, A. J., Woolnough, S. J., and Furtado, J. C.: How Do Stratospheric Perturbations Influence North American Weather Regime Predictions?, J. Climate, 35, 5915 – 5932, https://doi.org/10.1175/JCLI-D-21-0413.1, 2022.

https://doi.org/10.5194/egusphere-2024-2240
Preprint. Discussion started: 30 July 2024

Lee, S. H., Tippett, M. K., and Polvani, L. M.: A New Year-Round Weather Regime Classification for North America, J. Climate, 36, 7091 – 7108, https://doi.org/10.1175/JCLI-D-23-0214.1, 2023a.

Lee, S. H., Tippett, M. K., and Polvani, L. M.: Data for "A New Year-Round Weather Regime Classification for North America"[data set], https://doi.org/10.5281/zenodo.8165165, 2023b.

Leeding, R., Riboldi, J., and Messori, G.: On Pan-Atlantic cold, wet and windy compound extremes, Weather Clim. Extr., 39, 100 524, https://doi.org/10.1016/j.wace.2022.100524, 2023a.

Leeding, R., Riboldi, J., and Messori, G.: Modulation of North Atlantic extratropical cyclones and extreme weather in Europe during North American cold spells, Weather Clim. Extr., 42, 100 629, https://doi.org/10.1016/j.wace.2023.100629, 2023b.

Madden, R. A. and Speth, P.: The Average Behavior of Large-Scale Westward Traveling Disturbances Evident in the Northern Hemisphere Geopotential Heights, J. Atmos. Sci., 46, 3225 – 3239, https://doi.org/10.1175/1520-0469(1989)046<3225:TABOLS>2.0.CO;2, 1989.

Matsuno, T.: A Dynamical Model of the Stratospheric Sudden Warming, J. Atmos. Sci., 28, 1479 – 1494, https://doi.org/10.1175/1520-0469(1971)028<1479:ADMOTS>2.0.CO;2, 1971.

Matthewman, N. J., Esler, J. G., Charlton-Perez, A. J., and Polvani, L. M.: A New Look at Stratospheric Sudden Warmings. Part III: Polar Vortex Evolution and Vertical Structure, J. Climate, 22, 1566 – 1585, https://doi.org/10.1175/2008JCLI2365.1, 2009.

Matthias, V. and Kretschmer, M.: The Influence of Stratospheric Wave Reflection on North American Cold Spells, Mon. Weather Rev., 148, 1675 – 1690, https://doi.org/10.1175/MWR-D-19-0339.1, 2020.

Messori, G. and Faranda, D.: On the Systematic Occurrence of Compound Cold Spells in North America and Wet or Windy Extremes in Europe, Geophys. Res. Lett., 50, e2022GL101 008, https://doi.org/10.1029/2022GL101008, 2023.

Messori, G., Caballero, R., and Gaetani, M.: On cold spells in North America and storminess in western Europe, Geophys. Res. Lett., 43, 6620–6628, https://doi.org/10.1002/2016GL069392, 2016.

Messori, G., Kretschmer, M., Lee, S. H., and Wendt, V.: Stratospheric downward wave reflection events modulate North American weather regimes and cold spells, Weather Clim. Dynam., 3, 1215–1236, https://doi.org/10.5194/wcd-3-1215-2022, 2022.

Millin, O. T., Furtado, J. C., and Basara, J. B.: Characteristics, Evolution, and Formation of Cold Air Outbreaks in the Great Plains of the United States, J. Climate, 35, 4585 – 4602, https://doi.org/10.1175/JCLI-D-21-0772.1, 2022.

Nath, D., Chen, W., Wang, L., and Ma, Y.: Planetary wave reflection and its impact on tropospheric cold weather over Asia during January 2008, Adv. Atmos. Sci., 31, 851–862, https://doi.org/10.1007/s00376-013-3195-8, 2014.

Nath, D., Chen, W., Zelin, C., Pogoreltsev, A. I., and Wei, K.: Dynamics of 2013 Sudden Stratospheric Warming event and its impact on cold weather over Eurasia: Role of planetary wave reflection, Sci. Rep., 6, 24 174, https://doi.org/10.1038/srep24174, 2016.

Nishii, K.: Programs [code], https://www.atmos.rcast.u-tokyo.ac.jp/nishii/programs/index.html, 2016.

Perlwitz, J. and Harnik, N.: Observational Evidence of a Stratospheric Influence on the Troposphere by Planetary Wave Reflection, J. Climate, 16, 3011 – 3026, https://doi.org/10.1175/1520-0442(2003)016<3011:OEOASI>2.0.CO;2, 2003.

Perlwitz, J. and Harnik, N.: Downward Coupling between the Stratosphere and Troposphere: The Relative Roles of Wave and Zonal Mean Processes, J. Climate, 17, 4902 – 4909, https://doi.org/10.1175/JCLI-3247.1, 2004.

Plumb, R. A.: On the Three-Dimensional Propagation of Stationary Waves, J. Atmos. Sci., 42, 217 – 229, https://doi.org/10.1175/1520-0469(1985)042<0217:OTTDPO>2.0.CO;2, 1985.

Polvani, L. M. and Waugh, D. W.: Upward Wave Activity Flux as a Precursor to Extreme Stratospheric Events and Subsequent Anomalous Surface Weather Regimes, J. Climate, 17, 3548 – 3554, https://doi.org/10.1175/1520-0442(2004)017<3548:UWAFAA>2.0.CO;2, 2004.

https://doi.org/10.5194/egusphere-2024-2240
Preprint. Discussion started: 30 July 2024

Raghunathan, G. N. and Huang, H.-P.: An Updated Analysis of Northern Hemisphere Submonthly Retrograde Waves, Journal of the Atmospheric Sciences, 76, 3941 – 3954, https://doi.org/10.1175/JAS-D-19-0143.1, 2019.

Randel, W. J. and Held, I. M.: Phase Speed Spectra of Transient Eddy Fluxes and Critical Layer Absorption, J. Atmos. Sci., 48, 688 – 697, https://doi.org/10.1175/1520-0469(1991)048<0688:PSSOTE>2.0.CO;2, 1991.

Reichler, T. and Jucker, M.: Stratospheric wave driving events as an alternative to sudden stratospheric warmings, Weather Clim. Dynam., 3, 659–677, https://doi.org/10.5194/wcd-3-659-2022, 2022.

Renwick, J. A. and Wallace, J. M.: Relationships between North Pacific Wintertime Blocking, El Niño, and the PNA Pattern, Mon. Weather Rev., 124, 2071 – 2076, https://doi.org/10.1175/1520-0493(1996)124<2071:RBNPWB>2.0.CO;2, 1996.

Riboldi, J. and Schutte, M.: Space-time spectra of Northern Hemispheric Rossby waves during extended winter [data set], https://doi.org/https://snd.se/en/catalogue/dataset/preview/440eef3a-c462-458a-bdf1-b83e8c10b4f3/1, 2024.

Riboldi, J., Lott, F., D'Andrea, F., and Rivière, G.: On the Linkage Between Rossby Wave Phase Speed, Atmospheric Blocking, and Arctic Amplification, Geophys. Res. Lett., 47, e2020GL087 796, https://doi.org/10.1029/2020GL087796, 2020.

Riboldi, J., Rousi, E., D'Andrea, F., Rivière, G., and Lott, F.: Circumglobal Rossby wave patterns during boreal winter highlighted by space–time spectral analysis, Weather Clim. Dynam., 3, 449–469, https://doi.org/10.5194/wcd-3-449-2022, 2022.

Riboldi, J., Leeding, R., Segalini, A., and Messori, G.: Multiple Large-Scale Dynamical Pathways for Pan–Atlantic Compound Cold and Windy Extremes, Geophys. Res. Lett., 50, e2022GL102 528, https://doi.org/10.1029/2022GL102528, 2023.

Scherhag, R.: Die explosionsartigen Stratosphaerenerwärmungen des Spaetwinters 1951/52, Berichte des Deutschen Wetterdienstes in der US-Zone, 6, 51–63, 1952.

Schutte, M. K., Domeisen, D. I. V., and Riboldi, J.: Opposite spectral properties of Rossby waves during weak and strong stratospheric polar vortex events, Weather Clim. Dynam., 5, 733–752, https://doi.org/10.5194/wcd-5-733-2024, 2024.

Shaw, T. A. and Perlwitz, J.: The Life Cycle of Northern Hemisphere Downward Wave Coupling between the Stratosphere and Troposphere, J. Climate, 26, 1745 – 1763, https://doi.org/10.1175/JCLI-D-12-00251.1, 2013.

Shaw, T. A., Perlwitz, J., and Harnik, N.: Downward Wave Coupling between the Stratosphere and Troposphere: The Importance of Meridional Wave Guiding and Comparison with Zonal-Mean Coupling, J. Climate, 23, 6365 – 6381, https://doi.org/10.1175/2010JCLI3804.1, 2010.

Shaw, T. A., Perlwitz, J., and Weiner, O.: Troposphere-stratosphere coupling: Links to North Atlantic weather and climate, including their representation in CMIP5 models, J. Geophys. Res. Atmospheres, 119, 5864–5880, https://doi.org/10.1002/2013JD021191, 2014.

Shen, X., Wang, L., Scaife, A. A., Hardiman, S. C., and Xu, P.: The Stratosphere–Troposphere Oscillation as the Dominant Intraseasonal Coupling Mode between the Stratosphere and Troposphere, J. Climate, 36, 2259 – 2276, https://doi.org/10.1175/JCLI-D-22-0238.1, 2023.

Sjoberg, J. P. and Birner, T.: Transient Tropospheric Forcing of Sudden Stratospheric Warmings, J. Atmos. Sci., 69, 3420–3432, https://doi.org/10.1175/JAS-D-11-0195.1, 2012.

Sussman, H., Raghavendra, A., Roundy, P., and Dai, A.: Trends in northern midlatitude atmospheric wave power from 1950 to 2099, Clim. Dyn., 54, 2903–2918, https://doi.org/10.1007/s00382-020-05143-3, 2020.

Thompson, D. W. J. and Wallace, J. M.: Regional Climate Impacts of the Northern Hemisphere Annular Mode, Science, 293, 85–89, https://doi.org/10.1126/science.1058958, 2001.

Thompson, D. W. J., Furtado, J. C., and Shepherd, T. G.: On the Tropospheric Response to Anomalous Stratospheric Wave Drag and Radiative Heating, J. Atmos. Sci., 63, 2616–2629, https://doi.org/10.1175/JAS3771.1, 2006.

https://doi.org/10.5194/egusphere-2024-2240
Preprint. Discussion started: 30 July 2024

Wheeler, M. and Kiladis, G. N.: Convectively coupled equatorial waves: Analysis of clouds and temperature in the wavenumber–frequency domain, J. Atmos. Sci., 56, 374–399, https://doi.org/10.1175/1520-0469(1999)056<0374:CCEWAO>2.0.CO;2, 1999.

Wilks, D. S.: "The Stippling Shows Statistically Significant Grid Points": How Research Results are Routinely Overstated and Overinterpreted, and What to Do about It, B. Am. Meteorol. Soc., 97, 2263 – 2273, https://doi.org/10.1175/BAMS-D-15-00267.1, 2016.

Woollings, T., Hannachi, A., and Hoskins, B.: Variability of the North Atlantic eddy-driven jet stream, Q. J. Roy. Meteor. Soc., 136, 856–868, https://doi.org/10.1002/qj.625, 2010.